Materials Reports: Energy 3 (2023) 100175

Contents lists available at ScienceDirect

Materials Reports: Energy

journal homepage: www.keaipublishing.com/en/journals/materials-reports-energy

Review

Electrochemical CO_2 reduction: Progress and opportunity with alloying copper

Mao Ding [a,1], Zhaoyang Chen [a,1], Chunxiao Liu [a], Youpeng Wang [a], Chengbo Li [a], Xu Li [a], Tingting Zheng [a], Qiu Jiang [a,b,**], Chuan Xia [a,b,*]

[a] School of Materials and Energy, University of Electronic Science and Technology of China, Chengdu, 611731, PR China
[b] Yangtze Delta Region Institute (Huzhou), University of Electronic Science and Technology of China, Huzhou, 313000, PR China

ARTICLE INFO

Keywords:
Electrocatalysis
CO_2 reduction
Selectivity
Copper alloys
High-entropy alloys
Single-atom alloys

ABSTRACT

Electroreduction of carbon dioxide (CO_2) into value-added chemicals offers an entrancing approach to maintaining the global carbon cycle and eliminating environmental threats. A key obstacle to achieving long-term and large-scale implementation of electrochemical CO_2 reduction technology is the lack of active and selective catalysts. Copper (Cu) is one of the few candidates that can facilitate C–C coupling to obtain high-energy oxygenates and hydrocarbons beyond carbon monoxide (CO), but it suffers from poor selectivity for products of interest and high overpotentials. Alloying is an effective way to break the linear scaling relations and uniquely manipulate the reactivity and selectivity, which is hard to achieve by using monometallic compositions alone. By alloying Cu with other metals, one could change the catalytic properties of the catalyst by tuning the local electronic structure and modulating the adsorption strength of the reaction intermediates, thus improving the catalytic activity and selectivity. In this review, we focus on the recently developed Cu-based alloy catalysts (including conventional alloys, high-entropy alloys and single-atom alloys) that have been applied in electrocatalytic CO_2 reduction (ECR). Theoretical calculations and experimental advances in understanding the key rate-limiting and selectivity-determining steps in those alloys are summarized, with a particular focus on identifying binding energy descriptors and the dynamic product formation mechanisms. In addition, we outline the opportunities and challenges in the fundamental understanding of ECR by recommending advanced in-situ characterization techniques and standardized electrochemical methods and offer atomic-level design principles for steering the reaction pathways to the desired products.

1. Introduction

In recent years, the CO_2 concentration in the atmosphere has rapidly increased due to the excessive consumption of fossil fuels, resulting in a series of environmental problems, such as glacial melting, intensified natural disasters and global warming.[1–5] The "Paris Agreement" on climate change specifically stated the need to mitigate the greenhouse effect and control the global average temperature increase within 2 °C.[6,7] To achieve this goal, reducing CO_2 emissions and further seeking relevant practical technologies to convert them into industrial chemicals has become extremely urgent. Among various CO_2 conversion technologies, the electrochemical transformation of CO_2 into liquid fuels is one of the most promising methods to build carbon-neutral energy infrastructure due to its economic feasibility, operational simplicity and environmental compatibility.[8–12] As schematically illustrated in Fig. 1a, green electricity generated from renewable energy sources, such as wind, solar and hydroelectric power, can be combined with electrocatalytic CO_2 reduction (ECR) technology to immobilize CO_2 and convert it into

* Corresponding author. School of Materials and Energy, University of Electronic Science and Technology of China, Chengdu, 611731, PR China.
** Corresponding author. Yangtze Delta Region Institute (Huzhou), University of Electronic Science and Technology of China, Huzhou, 313000, PR China.
E-mail addresses: jiangqiu@uestc.edu.cn (Q. Jiang), chuan.xia@uestc.edu.cn (C. Xia).

Production and Hosting by Elsevier on behalf of KeAi

[1] These authors contributed equally to this work.

https://doi.org/10.1016/j.matre.2023.100175
Received 9 November 2022; Received in revised form 2 December 2022; Accepted 7 December 2022
Available online 10 January 2023

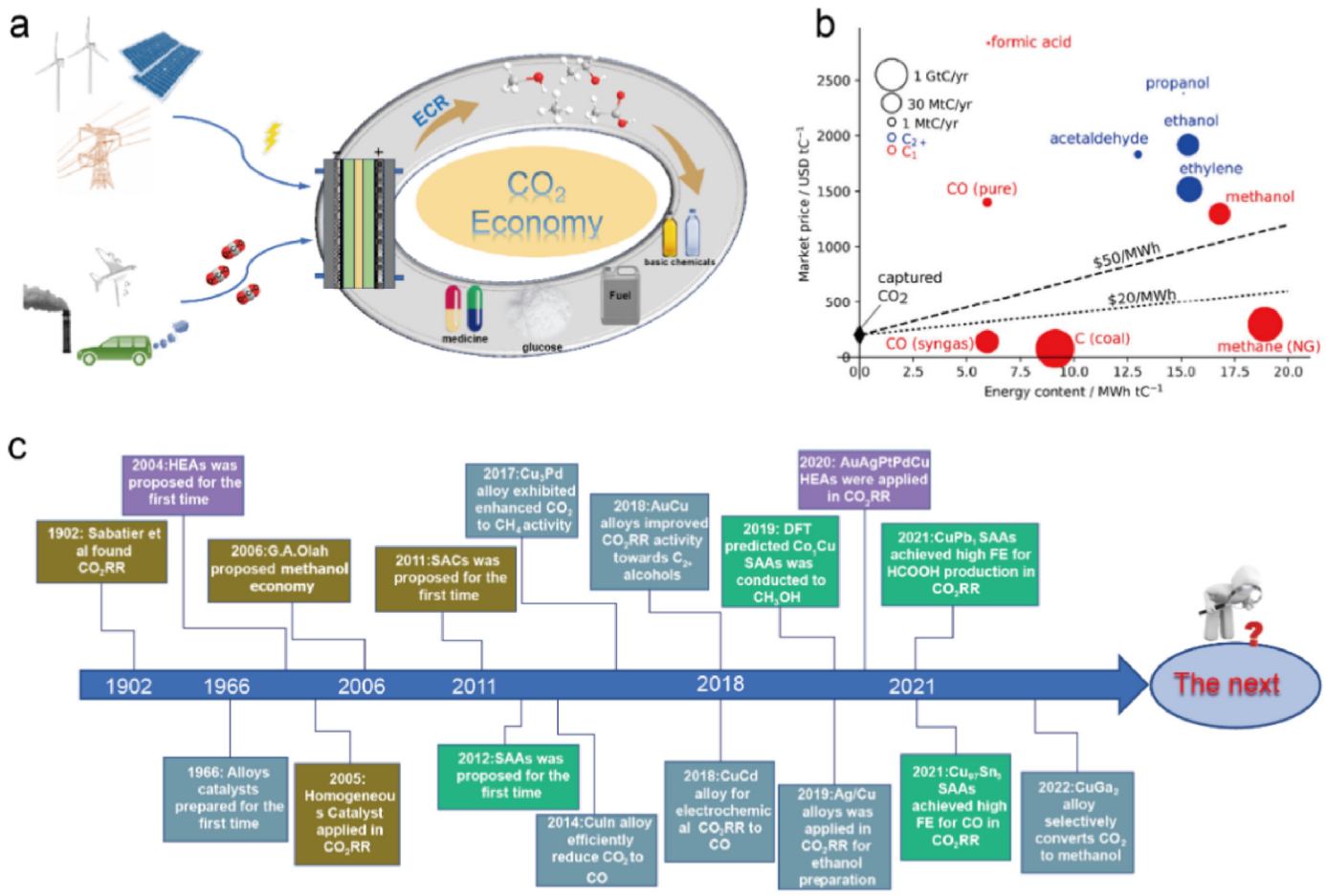

Fig. 1. (a) Schematic illustration of the carbon cycle via CO_2 electrolysis powered by renewable energy sources such as wind, solar and hydroelectric power. (b) Market price of select CO_2 recycling products as a function of energy content. Reproduced with permission from Ref. 13 (Lines represent minimum energy and CO_2 costs). (c) A timeline of the major development of Cu-based alloy and SAA electrocatalysts in carbon dioxide reduction.

easily available C_1/C_2 products, and autotrophic microorganisms are further used to produce value-added long-chain value-added chemicals. This technology can efficiently recycle CO_2 and store renewable electricity in chemical bonds in high-value chemicals. From the economic perspective, the energy content and value comparison of various chemicals in terms of their current market prices are summarized in Fig. 1b, which indicates that the products above the line for a given CO_2 capture cost and electricity cost may be economically feasible.[13]

To date, Cu is the most distinctive catalyst that shows appreciable faradaic efficiency for C–C coupling and has the ability to produce C_{2+} oxygenates and hydrocarbons.[14–18] This unique property is ascribed to the moderate adsorption of CO and weak binding with H, which encourage CO dimerization by suppressing the formation of CO, formic acid and H_2. In 2012, Jaramillo et al. used Cu material as a CO_2RR catalyst and obtained 16 different products from C_1 to C_3.[19] Although Cu possesses poor selectivity for a specific chemical, it is still the most effective catalyst for the deep reduction of CO_2 by more than two electrons. Since Masse et al. first synthesized a series of alloy catalysts (such as CuNi and CuPd), which display synergetic enhancement activity in the hydrogenation of benzene,[20] Cu-based alloy catalysts have been reported and widely used in the CO_2RR. Compared with monometallic catalysts, introducing foreign metal elements can either alter the electronic properties of the metal center or change the atom configurations at the active sites, so as to affect the adsorption energy and geometry of the intermediate. These effects may break the linear scaling relations and change the activity and selectivity of the catalysts.[21–24] Generally, metallic alloys can be formed by introducing one or multiple foreign metal elements into the host metal. The versatile choice of foreign elements provides rich exploration space for the design of alloy materials by changing their component ratios and arrangements. Although most studies focus on alloys containing two metal elements, high-entropy alloys (HEAs) containing more than five metal elements have recently attracted attention due to their high-entropy effect, lattice distortion, slow diffusion effect and cocktail effects.[25–29] In particular, after diluting the foreign metals across the host meal matrix as singly isolated sites, single atom alloys (SAAs) come into being, which exhibit peculiar electronic and geometric features distinct from their constituent metals. Integrating the advantages of single atoms and metal alloys, for example, due to the well-defined nature of the active sites and the unique alloying effects, SAAs have rapidly become a new research frontier and have shown remarkable potential in a wide range of catalytic reactions.[30–38] Nevertheless, similar to HEAs, the reported SAAs catalysts applied in ECR are rather rare, which awaits both opportunities and challenges. To gain an intuitive view of the development of this field, Fig. 1c displays a timeline of the major progress of Cu-based alloy, HEA and SAA electrocatalysts in ECR.

In this review, we described a systematic summary of the recent progress of Cu-based alloys, encompassing conventional Cu alloys, HEAs and SAAs for ECR applications. We also provide a mechanistic interpretation of the impact of catalyst composition and atomic arrangement on the reaction pathways and catalytic performance. Furthermore, we discuss future opportunities and challenges in Cu-based conventional alloys, HEAs and SAAs for the electrochemical conversion of CO_2 into value-added chemicals.

2. Pathways and mechanisms of CO_2 reduction

To date, a variety of CO_2RR reaction pathways have emerged, and up to 16 different products have been detected on Cu-based catalysts. Although it is possible to modify Cu-based alloys to target any one of these desirable products, we especially focused on the products that have been mostly reported, including various C_1 products (i.e., CO, formic acid (HCOOH), methanol (CH_3OH) and methane (CH_4)), C_2 products (i.e., ethylene (C_2H_4), ethane (C_2H_6), acetic acid (CH_3COOH), ethanol (CH_3CH_2OH)) and C_3 products (i.e., n-propanol ($CH_3CH_2CH_2OH$)). The standard reduction potentials for different ECR products are summarized in Fig. 2a. Among these products, HCOOH and CO are the simplest products that are formed via two proton-electron transfer reactions, and compete with each other. The selectivity is highly dependent on the initial absorption mode of the CO_2 molecules. For the CO pathway, carbon atom in the adsorbed CO_2 molecule is bonded to the catalyst surface, and the oxygen atom reacts with water and forms *COOH through a concerted proton-electron transfer process. Then, the adsorbed *COOH intermediate is reduced via another electron-proton transfer to form *CO and ultimately desorbed from the electrode.[39–41] For HCOOH formation, the two oxygen atoms in adsorbed CO_2 are bonded with the catalyst surface, causing the carbon atom in the adsorbed CO_2 to undergo hydrogenation and form HCOO*. HCOOH is finally obtained through further hydrogenation of HCOO* with either a surface *H or a proton in the electrolyte.[42,43]

The formation of other reported C_1 and C_{2+} hydrocarbons and oxygenates is generally considered to start with the same key intermediate *CO (Fig. 2b and c). Based on the catalytic properties and surface orientation of the catalyst, the *CO protonation process results in two possible products (*COH and *CHO), depending on the hydrogenation sites of oxygen or carbon, respectively. For *CHO formation, $*CH_2O$ can be generated from the proton-coupled electron transfer steps of *CO, which is the precursor for the formation of CH_4 following the reduction and dehydration steps.[44,45] Additionally, $*CH_2$ can be generated from the electron transfer and protonation steps of *CO in the *COH route, and CH_4 can be formed following another reduction and hydrogenation step from $*CH_2$.[46,47] Here, $*CH_2$ also serves as the selectivity determining intermediate to C_2H_6 and CH_3COO^-: if $*CH_2$ is further protonated to give the $*CH_3$ intermediate, two $*CH_3$ molecules can finally dimerize to form C_2H_6. However, the formation of CH_3COO^- involves a CO insertion mechanism.[48,49] *COH can be further protonated to form methanol. In the *COH route, it can be easily hydrogenated to form *CHOH, and the obtained *CHOH intermediate can be protonated again on the carbon site to form methanol.[46] For the other two products C_2H_4 and CH_3CH_2OH, the dimerization of *CO is the rate-determining step. The $OCCO^-$ formed by *CO dimerization can further undergo a series of electron transfer and protonation steps to form the $*CH_2CHO$ intermediate, which is further reduced to form C_2H_4 and CH_3CH_2OH.[50–52] The formation of the C_3 product mainly lies in stabilizing the key intermediates (such as CH_3CH_2O*), which can be further transformed to n-propanol via CO insertion and proton-coupled electron transfer processes (Fig. 2c).[53,54] Although this reaction mechanism seems reasonable for clarifying the formation of the C_3 product, almost no reactive intermediates of C_3 have been directly observed by in-situ characterization technology thus far. Therefore, challenges remain regarding how to constitute efficient ECR catalysts toward C_3 products and establish a descriptor between activity and electronic structure.

3. Cu-based conventional alloys in ECR

3.1. CuAg alloys

Alloying copper is an effective strategy to finely tune the composition and electronic properties of the alloy surface, which alters the reaction intermediate adsorption behavior and thus strengthens the reaction kinetics. Among various Cu-based alloys, Cu–Ag alloy systems have been developed because Ag is a CO-generating metal and can supply more CO to Cu. The increased coverage of the CO* intermediate on Cu sites could enhance the possibility of C–C coupling. For instance, Gewirth et al. prepared a homogeneously mixed nanoporous CuAg alloy catalyst by an additive-controlled electrodeposition method (Fig. 3a).[55] The optimal wire-like CuAg porosity alloy (CuAg-wire) displayed a higher *FE* for C_2H_4 (60%) and CH_3CH_2OH (25%) than the Cu-wire (40% and 20%, respectively) (Fig. 3b). In-situ Raman measurements indicate that such

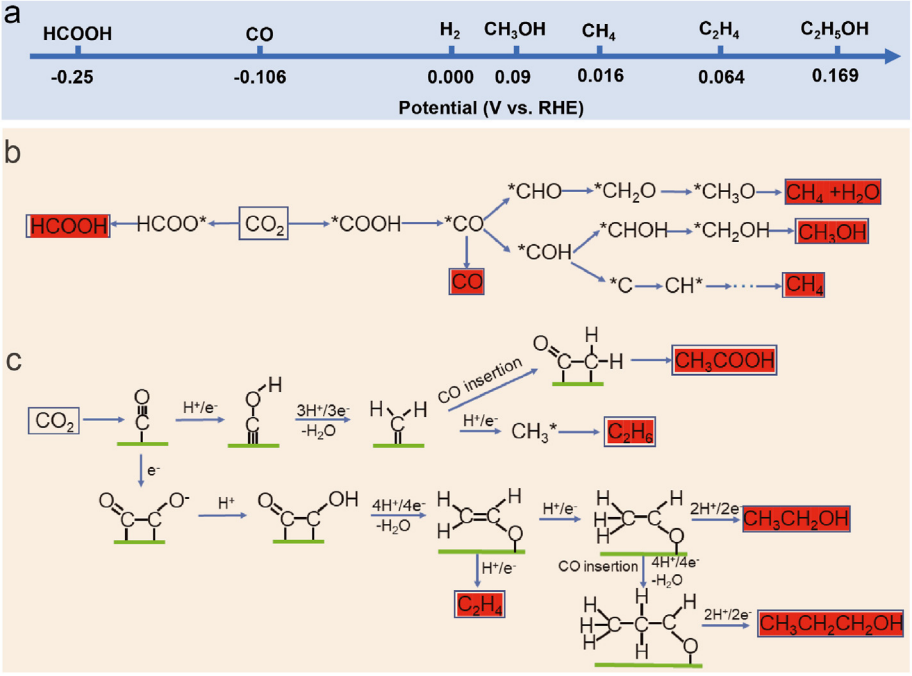

Fig. 2. (a) Standard reduction potentials for CO_2 electrolysis products. Reproduced with permission from Ref. 41. (b) Possible reaction pathways for CO_2 reduction to C_1 products. (c) Most likely C_{2+} pathways during ECR. Reproduced with permission from Ref. 48.

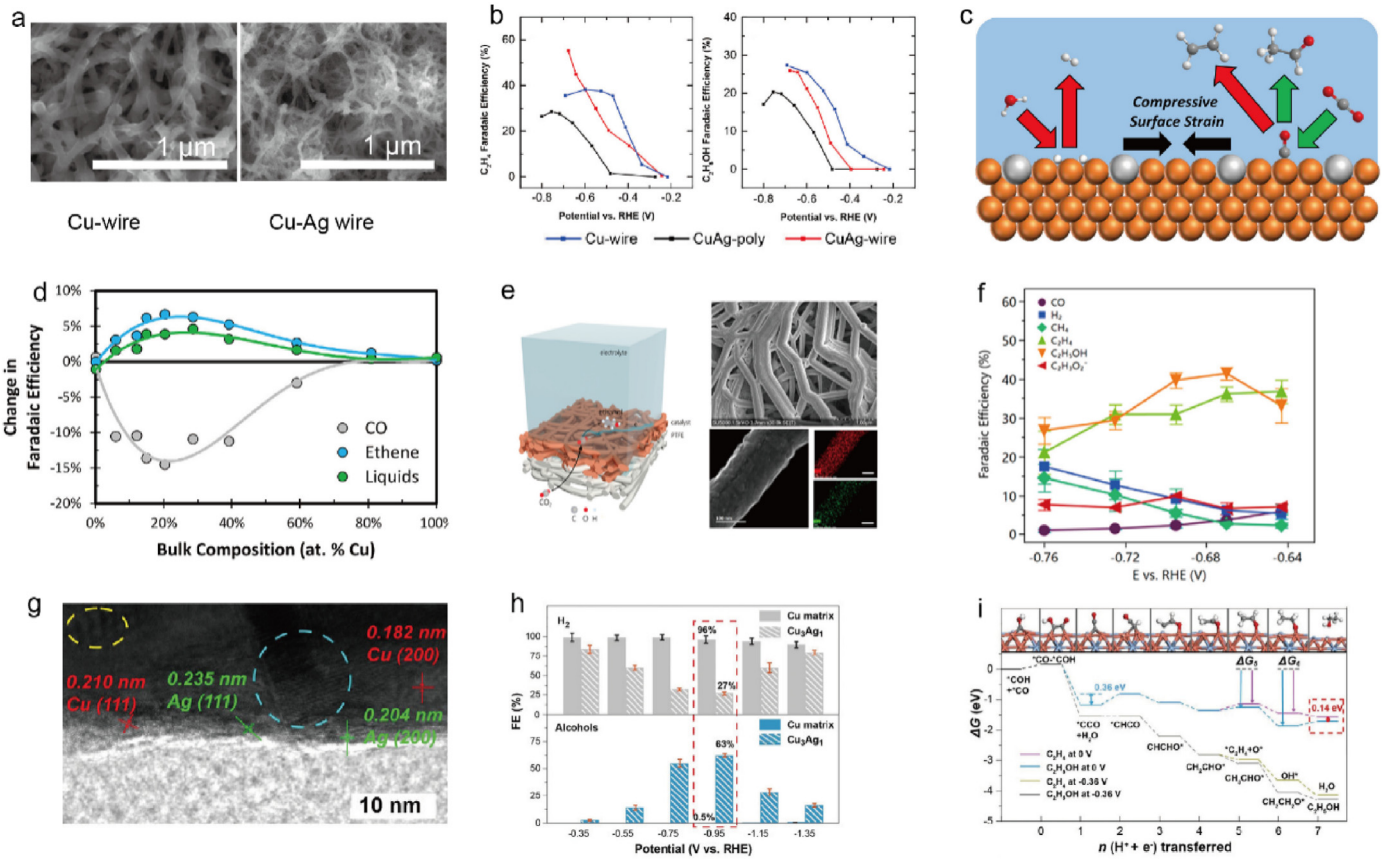

Fig. 3. Characterization and performance of the CuAg alloy catalyst for ECR. (a) SEM images of Cu-wire and Cu–Ag wire. (b) Faradaic efficiency of C_2H_4 and C_2H_5OH production. Reproduced with permission from Ref. 55. (c) Schematic illustration of the CuAg surface alloy causing compressive strain on the copper surface atoms. (d) Transient changes in the reaction selectivity observed over the CuAg electrodes at −1.05 V vs. RHE. Reproduced with permission from Ref. 56. (e) Schematic illustration of the catalyst electrode, SEM image, STEM image and EDX mapping of the $Ag_{0.14}/Cu_{0.86}$ catalyst. (f) Faradaic efficiency toward the major CO_2 reduction products. Reproduced with permission from Ref. 57. (g) HRTEM images of the Cu_3Ag_1 catalyst; (h) FE_{H2} and $FE_{alcohol}$ for ECR on the Cu matrix and Cu_3Ag_1 at different working potentials. (i) Free energy diagrams of *CO/*COH intermediate reduction to C_2 products. Reproduced with permission from Ref. 58.

enhanced activity mainly originates from the stable Cu_2O overlayer due to the alloying effect, after Ag is incorporated into Cu. Additionally, the optimal C_2H_4 selectivity can be further optimized by tuning the morphology and Ag loading. The distinctive activity and selectivity of alloy catalysts in ECR might be attributed to the change in their electronic and geometric structure. These variations further result in the enhanced binding strength for intermediates by shifting the *d*-band center. A typical investigation has shown that introducing silver to the copper surface to form a CuAg surficial alloy leads to compressive strains in the copper lattice. As a result, the electronic states of Cu changed, and the binding energies of hydrogen and oxygen were decreased, relative to CO (Fig. 3c), which led to an enhanced selectivity of C_2H_4 (Fig. 3d).[56]

In practical applications, ethanol, as a liquid fuel, has a high energy density (-1366.8 kJ mol^{-1}) and is also commonly used as a disinfectant with a volume fraction of 70%–75%. It also serves as a basic raw material for the further production of beverages, dyes and fuels.[59–63] Generally, it is easier to prepare C_2H_4 via ECR than CH_3CH_2OH over most Cu-based catalysts because conversion $*CH_2CHO$ to C_2H_4 has a lower energy barrier than $*CH_3CHO$ to CH_3CH_2OH.[64] Introducing an inert metal silver possessing weaker bonding ability to carbon could increase the diversity of binding sites and disrupt the active site configurations of intermediates for C_2H_4 production (Fig. 3e). In this case, the best catalyst, $Ag_{0.14}/Cu_{0.86}$ deposited on the PTFE substrate, was able to reduce CO_2 with the FE_{max} of 41% toward CH_3CH_2OH at a low overpotential of −0.67 V vs. RHE (Fig. 3f).[57] In-situ Raman spectroscopy revealed that the CO stretching peak on $Ag_{0.14}/Cu_{0.86}$ is much broader than that on pure Cu, which is mainly attributed to the diversity of binding configurations. Overall, this work demonstrates the multisite mechanism and alloying effect advantage of the AgCu catalyst and provides unique insights into designing other catalysts to promote ethanol production. Another intriguing work was reported by Zheng et al., in which they synthesized an electron-deficient Cu_3Ag_1 alloy catalyst by a galvanic replacement method.[58] Both twin boundaries (blue circle) and dislocations (yellow circle) coexist in the Cu_3Ag_1 alloy (Fig. 3g). These Cu_3Ag_1 catalysts with an electron-deficient state exhibited the FE_{max} of 63% for alcohol, outperforming the pure Cu matrix ($FE = 0.5\%$) (Fig. 3h). DFT calculations revealed that electron-deficient Cu sites in the Cu_3Ag_1 catalyst are capable of binding CH_3CHO* and CH_3CH_2O* intermediates in the alcohol pathway, resulting in its high catalytic selectivity for alcohol (Fig. 3i).

3.2. CuAu alloys

Au is a *d*-block metal and possesses good electrical conductivity, while it has a weak adsorption energy for hydrogen and oxygen.[65] Nanostructured Au is a state-of-the-art catalyst for catalyzing the CO_2-to-CO process, aside from its scarcity and low faradaic efficiency at high current densities.[66,67] Alloying Au with Cu has also been widely studied due to the synergistic effect, relatively weaker H-binding, compressive strain and grain boundary effects. These advantages can accelerate the formation of *COOH and favor CO* desorption from the electrode surface. For instance, Yang et al. demonstrated that catalytic properties can be accurately controlled by manipulating atomic arrangements.[68] As illustrated in Fig. 4a, CuAu alloys transformed from a

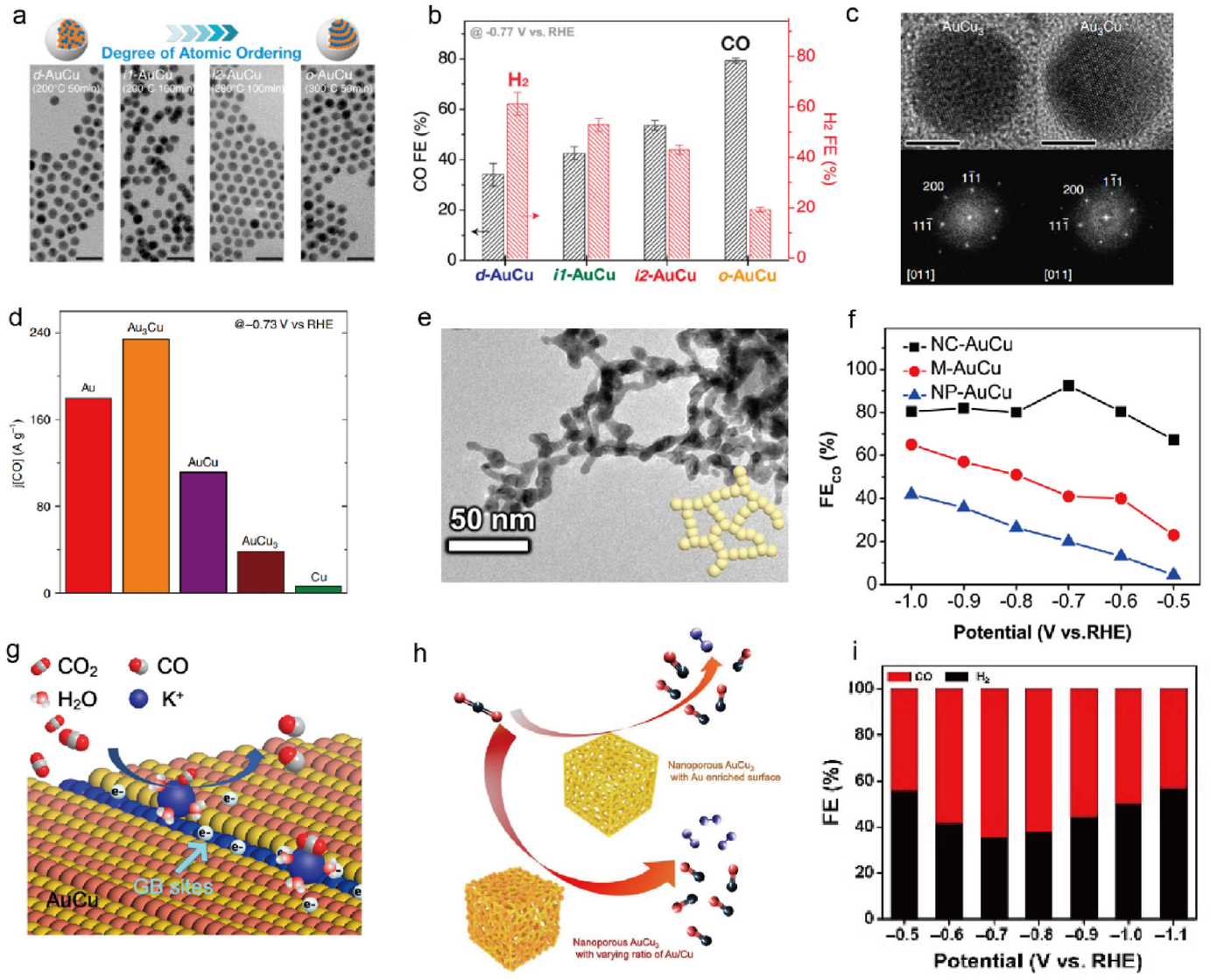

Fig. 4. Characterization and performance of the CuAu alloy catalyst for ECR. (a) TEM images of AuCu bimetallic NPs synthesized under various conditions (scale bar, 20 nm). (b) Electrochemical CO_2 reduction activities of AuCu bimetallic NPs (Measurements were conducted at −0.77 V vs. RHE with 0.1 M $KHCO_3$ solution). Reproduced with permission from Ref. 68. (c) HRTEM image of $AuCu_3$ and Au_3Cu and their fast Fourier transform (scale bar, 5 nm). (d) CO mass activity of Au–Cu bimetallic nanoparticles at −0.73 V vs RHE. Reproduced with permission from Ref. 69. (e) TEM images of the as-prepared AuCu aerogel. (f) CO Faradaic efficiency plots of NC-AuCu, M-AuCu and NP-AuCu catalysts. (g) Proposed schematic for CO_2 adsorption on grain boundaries. Reproduced with permission from Ref. 71. (h) Schematic illustration of the conversion of CO_2 to different products with various AuCu nanoporous alloys. (i) *FE* of ECR over $AuCu_3$-200. Reproduced with permission from Ref. 72.

disordered phase to an ordered structure by controlling the temperature and reaction time, wherein 300 °C and 50 min were the optimal parameters to produce highly crystallized CuAu alloys. As expected, the disordered CuAu alloys were more favorable for hydrogen evolution, whereas ordered CuAu NPs were efficient catalysts for CO_2-to-CO conversion (Fig. 4b). Mechanistic studies reveal that the increased selectivity of ordered CuAu is mainly attributed to the compression strain formed above the CuAu metallic intermetallic nucleus. Furthermore, manipulating alloy catalysts with high surface-to-volume or surface-to-mass ratio characteristics is more favorable for achieving high mass activity. Therefore, Yang et al. assembled two-dimensional CuAu bimetallic NPs with different compositions into ordered monolayers (Fig. 4c).[69] The Au_3Cu catalyst exhibited the highest mass activity toward CO, compared with the single-component Au or other component alloys (Fig. 4d). The synergy between the electronic effect and geometric effect in the Au_3Cu catalyst is conducive to CO evolution. Further inspection by DFT calculations demonstrated that the excellent activity of Au_3Cu can be attributed to the balance of the bonding of *COOH and *CO intermediates, which is effectively regulated by the local atomic arrangements in different surface compositions. At present, it is worth mentioning that the low efficiency in ECR may be caused by the limited concentration of CO_2 on the catalyst surface. Metal aerogels are rich in grain boundaries and have a large specific surface area, which is conducive to enriching the CO_2 concentration near the catalyst surface and in turn effectively promotes its catalytic activity.[70] The latest research shows that the local CO_2-enriched environment near the catalyst surface of the AuCu nanochain aerogel (NC–AuCu) is beneficial to enhancing the CO_2 to CO activity (Fig. 4e).[71] As a result, the NC-AuCu catalyst exhibits an *FE* of 92% for CO, outperforming those of the moderately aggregated AuCu (41%) and AuCu alloy nanoparticles (20%) (Fig. 4f). In-situ attenuated total reflection surface enhanced infrared absorption spectroscopy (ATR-SEIRAS) was performed at different potentials in 0.1 M CO_2-saturated $KHCO_3$ solution, showing an apparent peak at 2120 cm^{-1} assigned to *CO, which was intensified with the peak

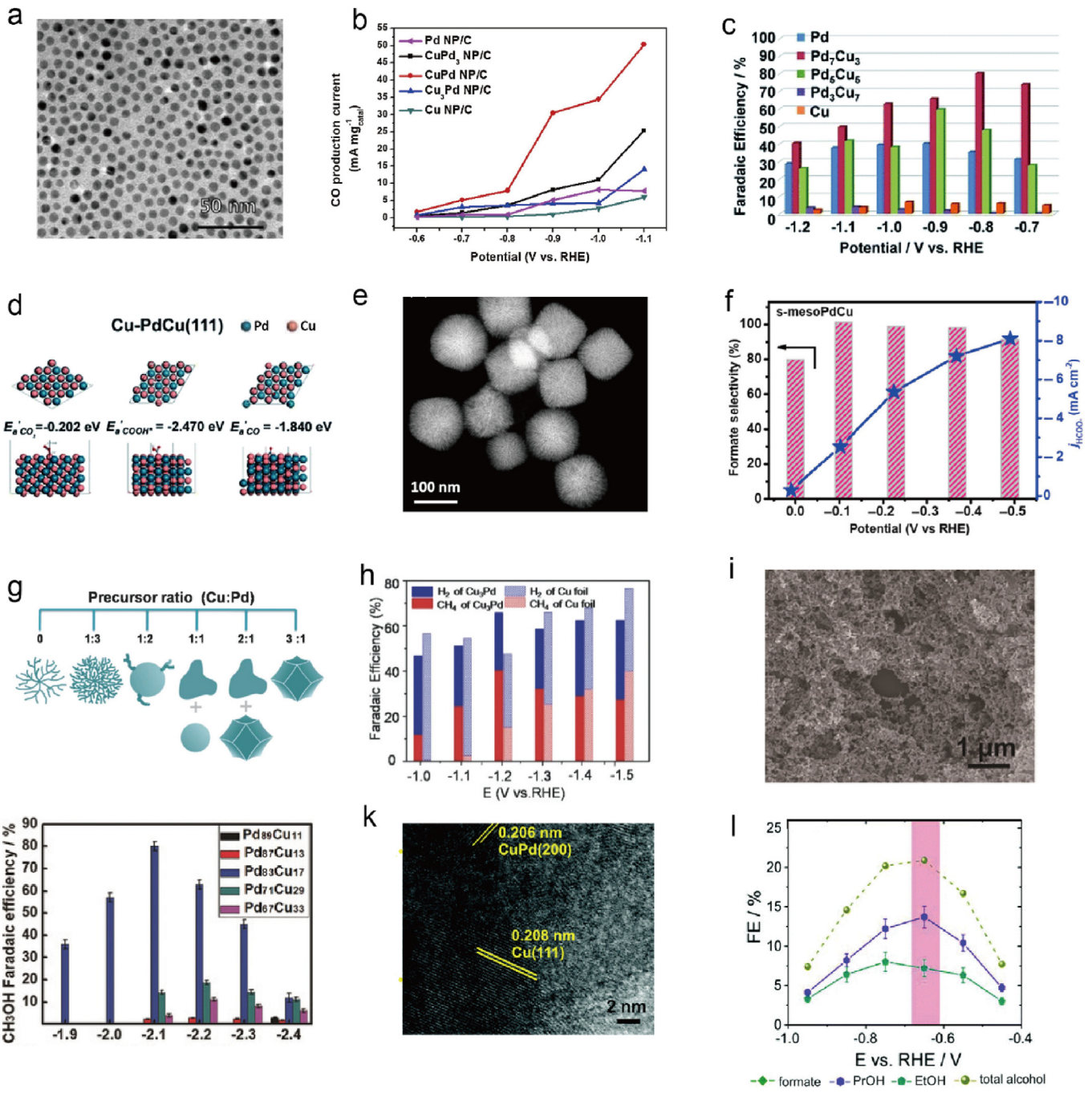

Fig. 5. Characterization and performance of the CuPd alloy catalyst for ECR. (a) TEM images of Cu_3Pd alloy NPs. (b) Partial current density of CO production, CO production current normalized by metal mass. Reproduced with permission from Ref. 75. (c) FE_{CO} of mesoporous Pd–Cu electrocatalysts. (d) Optimized geometries and adsorption energies for CO_2, *COOH intermediates and CO on the Cu-terminated Pd–Cu (111) facet. Reproduced with permission from Ref. 76. (e) STEM image of s-mesoPdCu nanocubes. (f) Potential-dependent formate selectivity and Faradaic efficiency of s-mesoPdCu. Reproduced with permission from Ref. 82. (g) Morphological evolution of Pd–Cu catalysts with different compositions. (h) CH_4 and H_2 *FE* of CRD-Cu_3Pd NCs and Cu foil. Reproduced with permission from Ref. 83. (i) SEM image of $Pd_{83}Cu_{17}$. (j) *FE* for CH_3OH over Pd_xCu_y aerogels. Reproduced with permission from Ref. 89. (k) TEM and HR-TEM analysis of the od-Pd_9Cu_{91} sample after pretreatment (45 min at −0.65 V vs. RHE). (l) Alcohol efficiencies derived from the electrolysis carried out over the od-Pd_9Cu_{91} sample, the pink bar graph represent a maximum selectivity of PrOH is observed at −0.65 V vs. RHE. Reproduced with permission from Ref. 94.

potential on NC-AuCu, demonstrating an efficient ECR to CO. The excellent catalytic activity is mainly attributed to the existence of GBs that can act as electron transfer channels to facilitate the accumulation of charges. This process can induce a strong local electric field to attract the cations (K^+) in the electrolyte, which adsorb CO_2 in turn, leading to local high concentrations of CO_2 (Fig. 4g). Among all CO_2 reduction products, the co-produced CO and H_2 (also called syngas) can be further transformed into liquid fuel via the well-studied Fischer-Tropsch reaction. In 2021, a simple air-heating aided method was reported to synthesize self-supporting nanoporous $AuCu_3$ alloys featuring both large specific surface area and flexible composition (Fig. 4h).[72] Driven by the concentration gradient under different temperatures, the surface compositions of Au and Cu can be adjusted, and controlled CO/H_2 composition can be achieved in a wide potential range within the range of −0.5 ~ −1.1V vs. RHE (Fig. 4i).

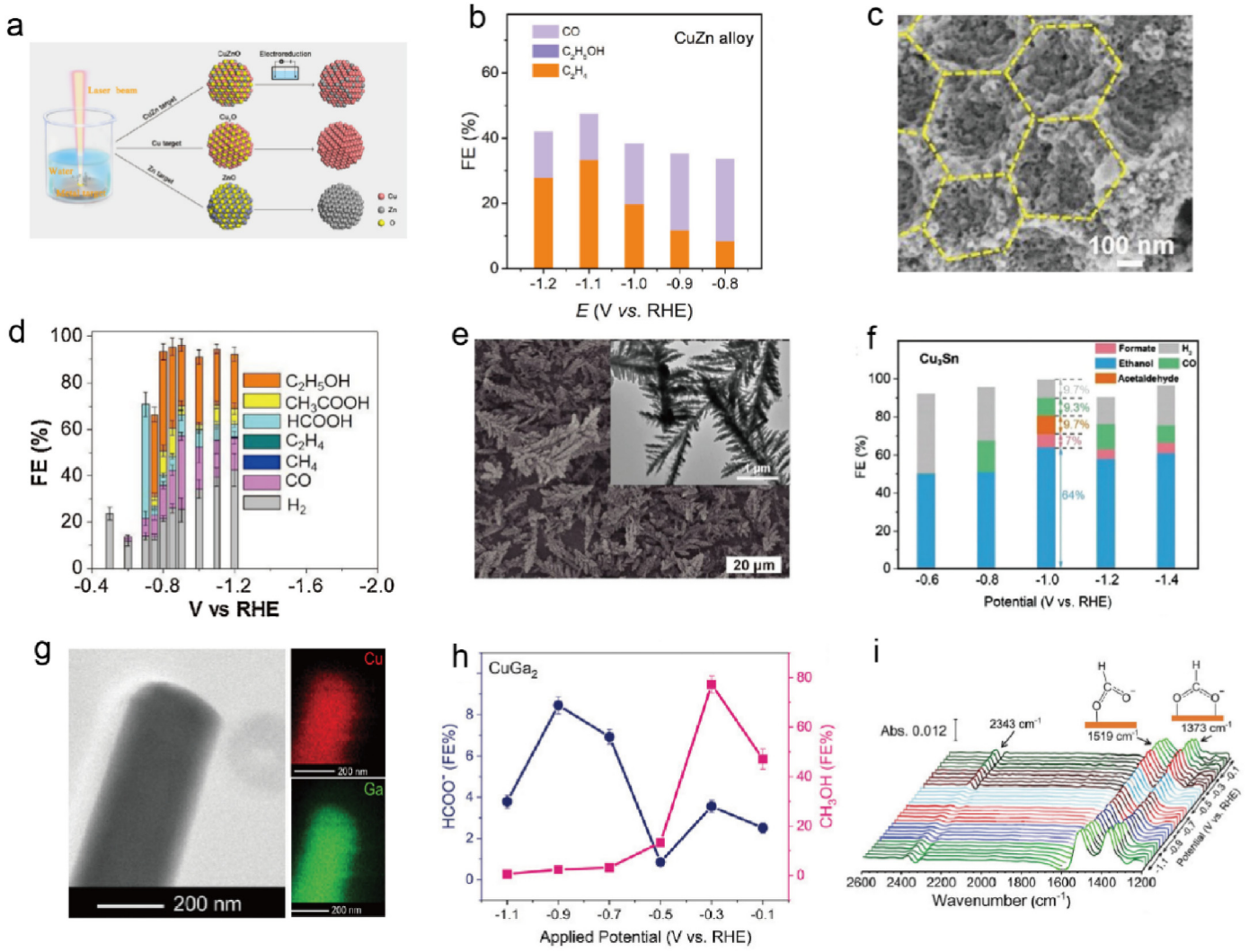

Fig. 6. Characterization and performance of Cu-based nonnoble metal alloy catalysts for ECR. (a) Schematic illustration of the preparation of CuZn, Cu and Zn NPs (The atomic ratio of Cu/Zn was 4:1). (b) *FE* values for ECR on CuZn alloy at different potentials. Reproduced with permission from Ref. 96. (c) high-magnification SEM images of Cu_5Zn_8. (d) *FE* of major products vs. potential for the Cu_5Zn_8 sample. Reproduced with permission from Ref. 97. (e) SEM and TEM (inset) images of Cu_3Sn. (f) Product distributions on Cu_3Sn at different potentials. Reproduced with permission from Ref. 98. (g) Low-resolution TEM image and elemental mapping of $CuGa_2$. (h) *FE* for each CO_2-reduced liquid product methanol and formate on $CuGa_2$. (i) In-situ IR spectra obtained during ECR using the $CuGa_2$ catalyst. Reproduced with permission from Ref. 88.

3.3. CuPd alloys

Pd is well known as a common mono-metallic catalyst for ECR that can generate either HCOOH or CO as the main products, which highly relies on the material microstructure, applied potential and alloying. Additionally, due to the easily poisoned characteristic of trace CO from ECR, Pd shows poor stability, especially at high overpotentials ($\eta > 200$ mV).[73,74] Combining these characteristics with a well-defined alloy nanostructure is a very promising scheme to obtain highly efficient ECR catalysts. For example, Lee et al. synthesized a series of monodispersed CuPd spherical shape alloy catalysts with the average diameter of ~6.6 nm (Fig. 5a).[75] Compared with single component Cu or Pd, all the CuPd alloy catalysts exhibited obviously increased CO mass activity (Fig. 5b). Furthermore, taking into account the energy barrier for CO* protonation, it was revealed that a well-designed alloyed surface can increase the energy barrier for the CO* protonation step and further suppress the formation of multicarbon products. In another example, it was found that both the alloying effect and elemental composition ratio affected the catalytic activity.[76] In the PdCu alloy system, when the content of Pd is higher than that of Cu, CO is the main reduction product (Fig. 5c). This study claimed that the activity increased mainly due to the significantly increased adsorption ability of the COOH* intermediate and CO* desorption ability on Cu-terminated PdCu (111) facets toward Pd (111) (Fig. 5d). Among the diversified products of ECR, HCOOH is one of the most economically profitable products regarding its market price and net electron utilization efficiency.[77–79] Furthermore, HCOOH is also widely used in pesticides, leather, pharmaceuticals and other industrial sectors.[80,81] In 2021, Liu et al. developed a soft-template method to prepare single-crystallinity PdCu alloy nanocubes (s-mesoPdCu) with abundant mesopores and cylindrical channels (Fig. 5e).[82] It was found that HCOOH was the main liquid-phase product, and almost negligible CO and H_2 were detected (Fig. 5f). The increase in selectivity and stability for s-mesoPdCu mainly arises from the electronic effect from alloying Pd with Cu, in which the intermediate binding energy can be effectively regulated by the *d*-band center. Additionally, the catalytic performance of the alloy catalysts for ECR varies with changes in their surface composition and structure. For example, even though the same initial element composition is chosen, different reduction products may be obtained, which highly depends on the slight variation of the above parameters. For instance, Gong et al. developed a one-pot wet-chemical

reduction method to synthesize high-index facet PdCu nanocrystals.[83] The morphology of the PdCu catalyst evolved from a uniform concave rhombic dodecahedron (CRD) to an irregular structure when adjusting the compositional ratio of Pd/Cu (Fig. 5g). A significantly increased *FE* of CH_4 was observed on the CRD Cu_3Pd alloy, which displayed the FE_{max} of CH_4 of approximately 40.6% at 1.2 V vs. RHE toward Cu foil (20.3%) (Fig. 5h). Density functional theory calculations suggest that combining the alloying effect with exposing low-coordination active sites is an efficient way to improve CO_2-to-CH_4 performance.

Methanol, as a high energy density liquid at room temperature, is deemed to be a more valuable C_1 product toward CO, HCOOH and CH_4. For example, combined with several mature industrial routes, methanol can transform into methylamine, dimethyl sulfate and pesticides.[84–87] Electrocatalytic conversion of CO_2 to CH_3OH is a multistep reaction process and has a higher Gibbs free energy ($\Delta G = -159.2$ kJ mol^{-1}).[88] To date, only a few catalysts can produce methanol through ECR. In 2018, Han et al. prepared a series of compositionally controllable Pd_xCu_y aerogel alloys with interconnected nanowires via a self-assembly method (Fig. 5i).[89] The ECR performance of $Pd_{83}Cu_{17}$ alloys was evaluated in an H-type cell with a 1-butyl-3-methylimidazolium tetrafluoroborate ([Bmim]BF4) aqueous solution as the electrolyte. As shown in Fig. 5j, the optimal ratio alloy ($Pd_{82}Cu_{17}$) shows the highest methanol *FE* of 80% at −2.1 V vs. Ag/Ag$^+$. The excellent activity of $Pd_{83}Cu_{17}$ alloys is mainly attributed to the synergistic effect of the special valence between Pd and Cu. This work indicates that the combination of a well-defined catalyst and specific electrolytes may offer a novel route for the preparation of methanol. However, it is unfortunate that when the catalyst was measured at 0.5 M $NaHCO_3$ and Na_2SO_4 aqueous solution, only H_2 and small amounts of formic acid was detected.

N-propanol is a valuable C_3 alcohol that possesses a high energy-mass density (30.94 kJ/g) and high octane number (118).[18,90] These unique characteristics endow n-propanol with great potential as an engine fuel. At present, n-propanol prepared by ECR conversion technology still suffers from low conversion efficiency ($FE_{n\text{-propanol}}$ <25%, partial current density<10 mA cm^{-2}). The greatest challenge in producing n-propanol with high selectivity for a catalyst is the lack of an effective active site stabilizing key C_2 intermediates to n-propanol and facilitating the coupling between C_1 and C_2.[59,91] Two different models are suggested for n-propanol formation (CO–CH_2CHO and CO–OCCO).[53,92,93] As an example, Broekmann et al. developed a dynamic hydrogen bubble template approach to synthesize a binary PdCu alloy dendritic structure foam (Fig. 5k).[94] The optimal ratio state Pd_9Cu_{91} foam exhibited an improved *FE* (13.7%) for n-propanol in 0.5 M $KHCO_3$ solution at −0.65 V vs. RHE, with a partial current density of −1.15 mA cm^{-2} (Fig. 5l). Mechanistic analysis revealed that *CO and *H first formed at Pd-rich PdCu sites and then concertedly spilled over to the Cu-rich domain. n-Propanol was further formed via another *CO binding to the stabilized *$CHCH_3$ intermediates.

3.4. Cu-based other nonnoble metal alloys

In addition to alloying precious metals, many efforts have been devoted to developing Cu-based nonprecious metal alloy catalysts for ECR because of their relatively inexpensive and nontoxic characteristics. For instance, Zn has low HER activity and high CO selectivity in ECR.[95] Therefore, it is anticipated that combining Zn with Cu can suppress the HER reaction and promote the adsorption of *CO intermediates, further facilitating C–C coupling on the Cu sites. Du et al. reported highly homogeneous CuZn alloys by laser ablation technology (Fig. 6a).[96] Indeed, the CuZn alloy catalyst exhibited the highest *FE* of 33.3% toward C_2H_4 at a potential of −1.1 V vs. RHE in ECR (Fig. 6b) and maintained the performance for 16 h of continuous electrolysis. Further mechanism analysis revealed that Cu and Zn atoms uniformly distributed on the surface of the alloy, which were capable of stabilizing the CO* intermediate and dimerization, resulting in excellent performance for the C_2H_4 product. Since the deep reduction product via ECR is kinetically unfavorable, prolonged retention time of the intermediates by the abundant pores is an effective way to obtain hydrocarbon products. Porous nanostructure alloy materials not only have a unique electronic or geometric structure showing a relatively long retention time of the intermediates, but can also maintain the localized pH value unchanged. Fig. 6c shows tightly packed hexagons hierarchically in the CuZn alloy catalysts, which delivers a high ethanol *FE* of 46.6% at −0.8 V vs. RHE with a specific current density of 2.3 mA cm^{-2} in aqueous solution (Fig. 6d).[97] The excellent activity was ascribed to the alloying effect and synergistic, structural and compositional advantages.

Recently, the concept of entropy was introduced in binary alloys, and corresponding research shows that high entropy state Cu_6Sn_5 alloys are unfavorable for *CO adsorption. Under this trend, a dendritic morphology low-entropy state Cu_3Sn alloy catalyst was reported for the effective conversion of CO_2 to ethanol (Fig. 6e).[98] From the ECR test at the optimal potential (−1.0 V vs. RHE), Cu_3Sn exhibited outstanding selectivity for ethanol (~64%) compared with electrodeposited Sn (<1%) or Cu (<5%) (Fig. 6f). First-principles calculations reveal that low-entropy Cu_3Sn is essential to the adsorption and stabilization of key intermediates (*CO and *CHCHOH) in the CO_2-to-ethanol pathway. Further life-cycle assessment showed that high ECR performance toward ethanol can reduce carbon emissions by 55%, compared to the traditional bioethanol process. To date, there are still great challenges in preparing methanol solution by ECR in traditional aqueous electrolytes (such as $KHCO_3$ or KCl). In 2022, C. Peter et al. developed a high-temperature solid-state method to synthesize $CuGa_2$ and Cu_9Ga_4 catalysts (Fig. 6g).[88] The ECR test was carried out for both above catalysts in 0.5 M $KHCO_3$ aqueous solution. $CuGa_2$ achieved a highest methanol *FE* of 77.26% at a low reduction potential of −0.3 V vs. RHE in contrast with Cu_9Ga_4 (*FE* of 37.75% at −0.1 V vs. RHE) (Fig. 6h). To further elucidate the CO_2-to-CH_3OH mechanism over the $CuGa_2$ catalyst, in-situ attenuated total reflection Fourier transform infrared (ATR-FTIR) measurements were conducted. As illustrated in Fig. 6i, applying a potential from −0.1 to −1.1 V vs. RHE over $CuGa_2$, two prominent peaks can be observed at 1519 cm^{-1} and 1373 cm^{-1}, which correspond to the asymmetric and symmetric stretching of the OCO group in $HCOO^-$. The adsorbed H at the Cu site can spill over to the Ga site and then further react with the adsorbed formic acid intermediate to form methanol. In addition, other nonnoble metals, such as In, Sb and Co, alloying with Cu were also explored for ECR.

4. Cu-based HEAs in ECR

Recently, as a new type of multifunctional alloy catalyst, HEAs have sparked much research interest, due to their excellent mechanical properties, sluggish diffusion effects and superior stability characteristics.[99–101] Generally, HEAs are defined as alloys with five or more principal elements.[102] Compared to conventional alloys, HEAs can break through the limitation of the large immiscible gap of elements by generating more stable intermetallic compounds. In addition, the finely tuned surface geometry is equipped with the ability to maximize the adsorption sites for intermediates.[29,103] More intriguingly, owing to the severe lattice distortion by atomic size mismatch, HEAs can take on the thermodynamically nonequilibrium state, which in turn leads to a lower energy barrier toward the catalytic reaction process.[104] These unique electronic and geometric characteristics make HEAs a versatile platform for the construction of catalysts with unexpected catalytic properties. However, to date, very few studies have reported using HEAs as ECR catalysts. The only experimental study we have found was reported in 2020, in which Biswas et al. prepared cryomilled nanocrystalline equiatomic AuAgPtPdCu HEAs by a low-temperature ball milling method for ECR application. As shown in Fig. 7a, the Cu atoms are stabilized by other metals in “FCC-facet” crystal structures.[105] The atom probe tomography (APT) indicated that all elements are uniformly distributed in the single-phase FCC matrix (Fig. 7b). Remarkably, the HEA catalyst exhibited an optimal *FE* for the predominant products CH_4 (49.4%) and

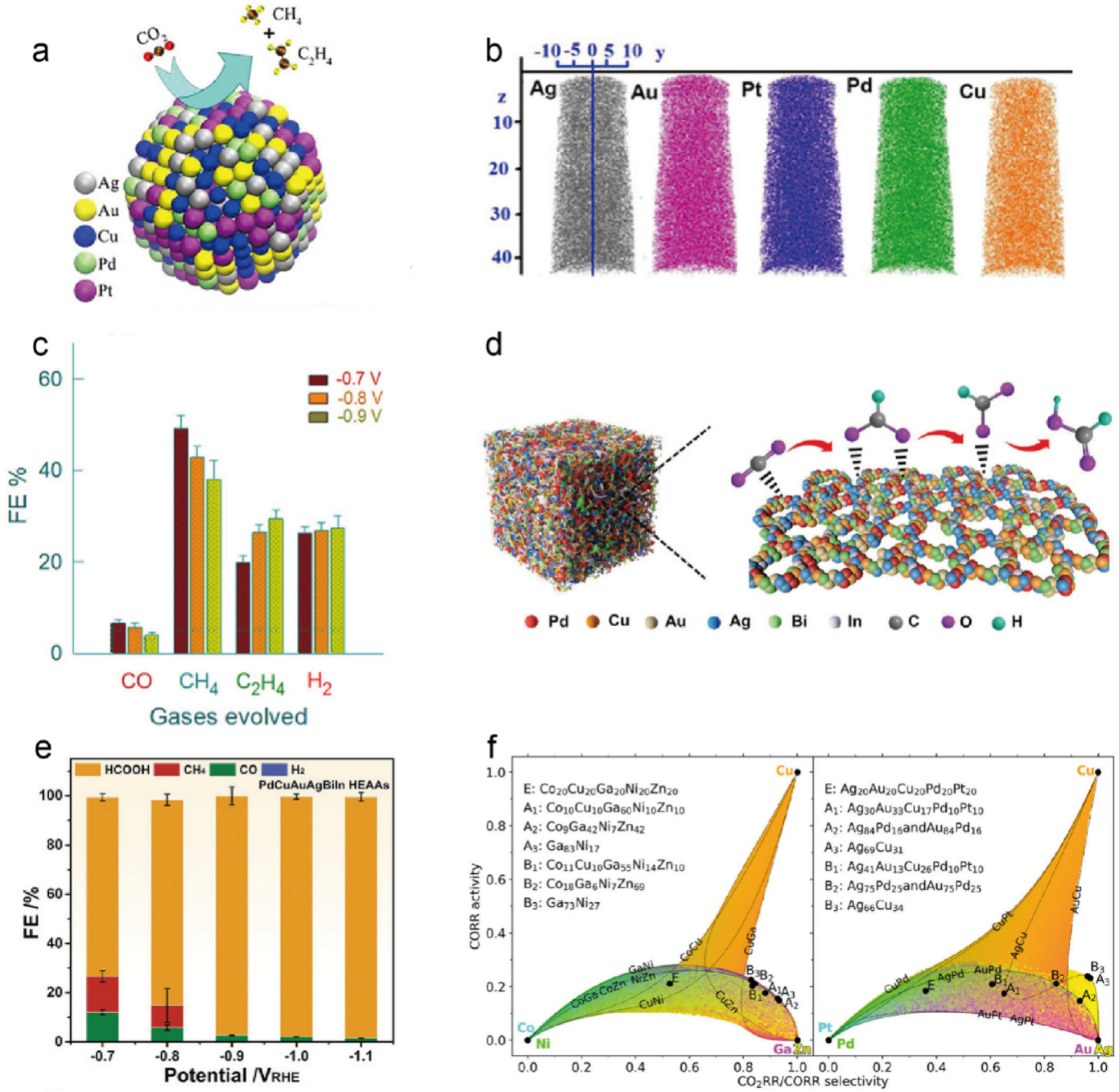

Fig. 7. Characterization and performance of Cu-based high-entropy alloy catalysts for ECR. (a) Schematic of the catalytic reaction demonstrated in the current work. (b) Chemical homogeneity of Au, Ag, Pt, Pd and Cu (mapping of an atom probe microscope). (c) Faradic efficiencies of their respective carbonaceous species and hydrogen gaseous products. Reproduced with permission from Ref. 105. (d) Schematic for boosted HCOOH generation over PdCuAuAgBiIn HEAs. (e) *FE* of major products vs. potential for the PdCuAuAgBiIn sample, reproduced with permission from Ref. 106. (f) Selectivity-activity plots of the CO_2RR/CORR selectivity and CORR activity space achievable by CoCuGaNiZn (left) and AgAuCuPdPt (right). Reproduced with permission from Ref. 107.

C_2H_4 (19.9%) at −0.7 V vs. RHE (Fig. 7c), which is attributed to the destabilization of the intermediate *OCH_3 and stabilization of the *O intermediate on the HEA surfaces. Another example is the PdCuAuAgBiIn HEA aerogels prepared by Liu et al., which showed outstanding catalytic performance for CO_2 reduction to HCOOH in a $KHCO_3$ aqueous electrolyte (Fig. 7d). At −1.1 V vs. RHE, the *FEs* of HCOOH products reached 98.1%, outperforming those of the PdCuAuAgBiIn high-entropy alloy particles and Pd metallic aerogels (Fig. 7e). The authors attributed this extraordinary electrocatalytic activity to the strong interactions between different metals and surface unsaturated sites in PdCuAuAgBiIn HEAs.[106]

These two research efforts open the door to the field of ECR about HEAs, and thus it is believed that more meaningful research work will be conducted in the future. Another theoretical work was conducted by Rossmeisl et al., who combined DFT with a supervised machine learning method to predict selective and active ECR catalysts on HEAs. Specifically, CoCuGaNiZn and AgAuCuPdPt HEAs were chosen as the optimal structural models, and the related local optimal disordered compositions are displayed in Fig. 7f.[107] The authors proved that this model allows the prediction of effective candidate catalysts without prior knowledge of their catalytic performance. As ECR undergoes pathways involving more

complex intermediates beyond *CO, it remains a biased and nascent topic for the prediction of ECR properties for disordered HEAs. Therefore, more experimental and theoretical studies are urgently needed to elucidate the influence of various HEAs on CO_2 reduction, and these disparate observations can be further combined for more consistent conceptual guidance.

5. Cu-based SAAs in ECR

Amalgamating the advantages of both heterogeneous and homogeneous catalysts, SAA catalysts with well-defined coordination environments provide an ideal model platform for structure-activity relationship studies. Usually, Cu-based SAAs can exhibit some unexpected catalytic features, such as anti-toxicity and adjustable reaction pathways. A typical example is exemplified by Pt_1Cu SAAs, where CO binds more weakly to Pt in Pt_1Cu SAAs in comparison to monometallic Pt, enabling Pt_1Cu SAAs to be excellent CO-tolerant catalysts for large-scale applications.[108] In addition, other Cu-based SAAs (such as Ni_1Cu, Pd_1Cu, Rh_1Cu, etc.) have been reported and applied in various catalytic fields.[109–111] Nevertheless, the application of SAAs in the ECR field is still in its infancy. Only a few studies on Cu-based SAAs have been reported. For example, Zhao et al. reported isolated Sn atoms on a metal Cu surface ($Cu_{97}Sn_3$) through a simple one-step coreduction method.[112] The $Cu_{97}Sn_3$ SAAs exhibited excellent selectivity to CO over a wide range of potentials (Fig. 8b), where the bulk alloy ($Cu_{70}Sn_{30}$) was switched to HCOOH as the main product. DFT calculations reveal that Cu–Sn SAAs possess a much lower

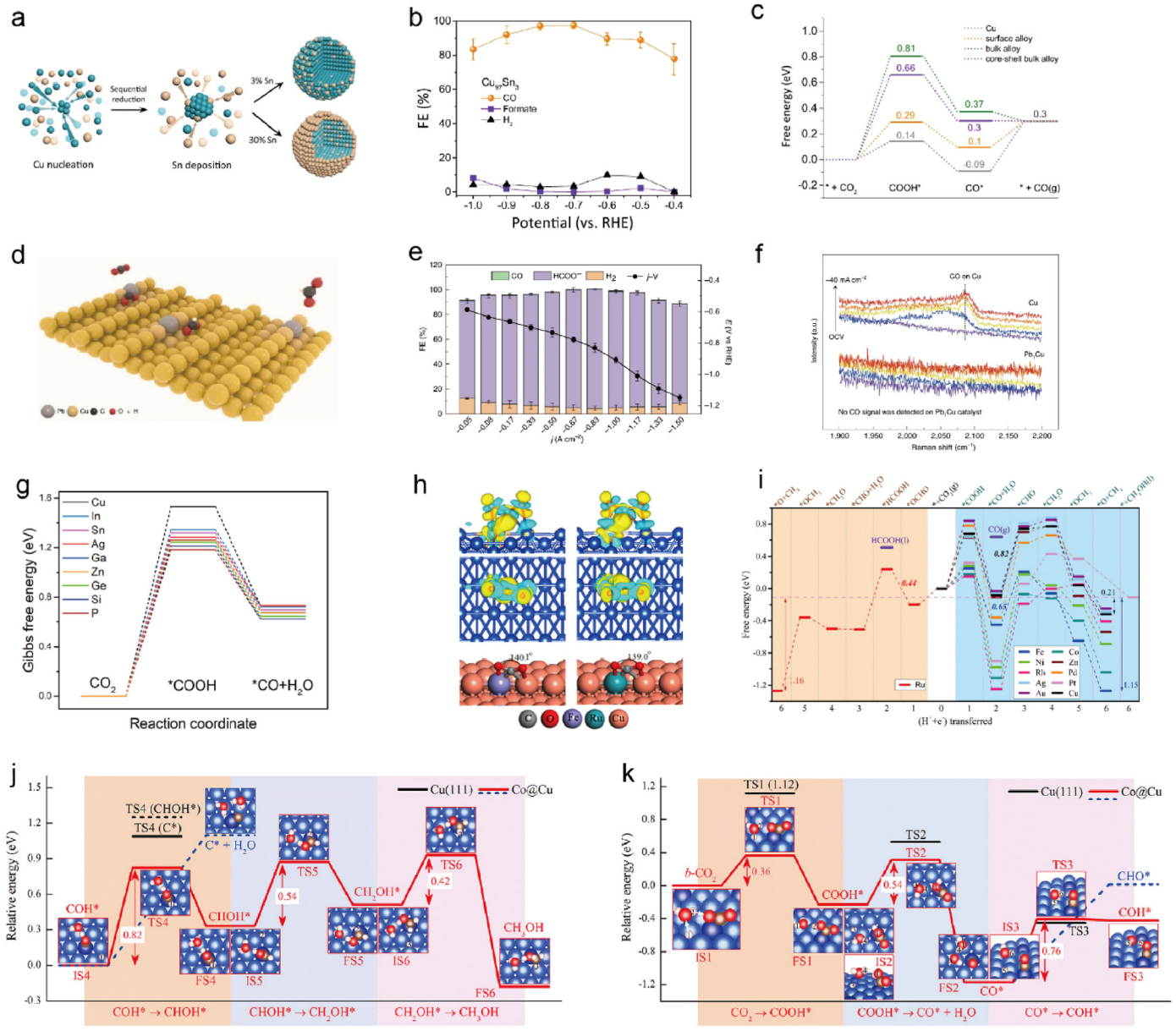

Fig. 8. Characterization and performance of Cu-based SAA catalysts for ECR. (a) Schematic illustration of the preparation of the Cu–Sn alloy ($Cu_{70}Sn_{30}$ and $Cu_{97}Sn_3$). (b) Faradaic efficiencies at various potentials of $Cu_{97}Sn_3$. (c) Calculated free energy diagrams of CO_2-to-CO conversion, reproduced with permission from Ref.112. (d) Schematic illustration of CO_2 conversion into HCOOH over a Pb_1Cu SAA. (e) *FE* of all ECR products at different current densities and the corresponding *j-v* curve. (f) In-situ Raman spectra recorded at different current densities. Reproduced with permission from Ref. 113. (g) Gibbs free energy diagrams of CO_2 reduction toward *CO on Cu-based SAAs. Reproduced with permission from Ref. 114. (h) isosurface of the charge density difference for CO_2 adsorbed on Fe@Cu (left) and Ru@Cu (right). (i) Free energy profiles for the preferential ECR pathway on M@Cu (211), leading to CH_4 or CH_3OH formation at 0 V (vs. RHE), Reproduced with permission from Ref. 115. (j) Relative energy diagram for the reduction of b-CO_2 to COH* and (k) COH* to CH_3OH on Co@Cu under zero voltage. Reproduced with permission from Ref. 116.

Table 1
Performance summary of recent reports on Cu-based alloy materials.

ECR	Electrocatalyst	Electrolyte	Potential	FE/%	Current density (mA cm^{-2})	Ref.
CO	AuCu	0.1 M $KHCO_3$	−0.77 V vs. RHE	80	−1.74	68
	Au_3Cu	0.1 M $KHCO_3$	−0.73 V vs. RHE	65	−3	69
	NC-AuCu	0.1 M $KHCO_3$	−0.21 V vs. RHE	~95	~ −30.10	71
	CuPd	0.1 M $KHCO_3$	−0.90 V vs. RHE	87	N.A.	75
	Pd_7Cu_3	0.1 M $KHCO_3$	−0.80 V vs. RHE	80	~-1	76
	CuIn	0.1 M $KHCO_3$	−0.50V vs. RHE	90	~ −0.50	119
	$Cu_{97}Sn_3$(F)	1.0 M KOH	−0.45 V vs. RHE	87	−100	112
HCOOH	$Pd_{82}Cu_{18}$	0.1 M $KHCO_3$	−0.30 V vs. RHE	96	~ −4.80	120
	s-meso PdCu	0.1 M $KHCO_3$	−0.11 V vs. RHE	100	~ −2.40	82
	SnCu	0.5 M KCl	−1.14 V vs. RHE	~96	−82.30 ± 2.10	121
	$In_{1.5}Cu_{0.5}$	0.1 M $KHCO_3$	−1.20 V vs. RHE	90	~ −5.60	122
	$Cu_{90}Co_{10}$	0.1 M $KHCO_3$	−1.10 V vs. RHE	10	~-21	123
	Pb_1Cu(F)	0.5 M $KHCO_3$	−0.90 V vs. RHE	96	−1000	113
CH_4	CRD-Cu_3Pd	0.1 M $KHCO_3$	−1.20 V vs. RHE	40.6	~ −9.40	83
	AuAgPtPdCu	0.5 M K_2SO_4	−0.70 V vs. RHE	49.4	−6.83	105
CH_3OH	$CuGa_2$	0.5 M $KHCO_3$	−0.30 V vs. RHE	77.3	~ −2.00	88
	$Pd_{83}Cu_{17}$ aerogel	[Bmim]BF_4 aqueous solution	−2.10 V vs. Ag/AgCl	80	−31.80	89
C_2H_4	CuAg wire(F)	1 M KOH	−0.70 V vs. RHE	60	−300	55
	$Cu_{10}Sb_1$	0.1 M KCl	−1.19 V vs. RHE	49.7	−28.50	124
	CuZn	0.1 M $KHCO_3$	−1.10 V vs. RHE	33.3	−6.10	96
C_2H_5OH	$Ag_{0.14}/Cu_{0.86}$(F)	1 M $KHCO_3$	−0.67 V vs. RHE	41	−250	57
	Cu_5Zn_8	0.1 M $KHCO_3$	−0.80 V vs. RHE	46.6	~ −5.10	125
	Cu_3Sn	0.1 M $KHCO_3$	−1.00 V vs. RHE	64	~ −9	98
	Cu_3Ag_1	0.5 M $KHCO_3$	−0.95 V vs. RHE	63	−25	58
C_3H_7OH	Pd_9Cu_{91} foam	0.5 M $KHCO_3$	−0.65 V vs. RHE	13.7	~ −8.39	94

Note: F represents the catalyst test via flow cell; others were measured by H-cell.

free energy of CO* (0.1 eV) formation toward HCOOH (0.38 eV), indicating that COOH* is more inclined to reduce to CO* than HCOOH. On the pure Cu surface, however, the strong absorption of CO* (−0.09 eV) tends to form C_2H_4. With regard to both Cu–Sn bulk and core-shell alloys, the free energy of COOH* increased to 0.66 eV and 0.81 eV. This result clarified the CO formation toward Cu–Sn SAAs. Similar results were also reported by Huang et al., who synthesized a series of Cu–Sn composite catalysts ($Cu_{20}Sn_1$ and Cu_1Sn_1) via a simple coreduction method.[24] The results show that high *FE* of 95.3% for CO and 95.4% for HCOOH were achieved on the $Cu_{20}Sn_1$ and Cu_1Sn_1 catalysts, respectively.

Currently, large-scale implementation ECR still faces a series of technical obstacles, especially the subsequent separation and purification problems of liquid products. Recently, our group reported that a single-atom Pb alloyed Cu catalyst (Pb_1Cu) can achieve pure formic acid production with a solid electrolyte reactor (Fig. 8d–f).[113] In this case, HCOOH, as the only liquid product, displayed the highest *FE* of 96% with a current density of −800 mA cm^{-2}. Such activity is the best among the previously reported formic acid electrocatalysts. Moreover, 0.16 M pure HCOOH solution can also be achieved at approximately −3.86 V by a solid electrolyte reactor system. To identify the catalytic mechanism and determine the absorbed surface intermediates, in-situ Raman spectra for Cu and Pb_1Cu SAA were obtained. It shows an obvious *CO signal on the Cu catalyst and the absence of CO formation on the Pb_1Cu catalyst surface. As noted above, *CO is the key intermediate for the formation of C_{2+} products. Therefore, this result strongly implies that alloying (introducing Pb atoms on the copper surface) can significantly inhibit the occurrence of C–C coupling. This work not only offers new insights into the role of the surface alloying effect in manipulating the priority path, but also provides a reliable design route for SAAs.

At present, experimental research on copper-based SAAs for ECR is still in the nascent stage, and catalyst development usually follows a "trial and error" strategy. Therefore, more efficient catalyst design through theoretical learning guidance will be a very meaningful research direction. For instance, Zou et al. took Cu-based SAAs as the starting model, using the machine learning method to demonstrate that the valence electron number and low generalized coordination numbers are two main factors for ECR.[114] Furthermore, the detailed Gibbs free energy diagrams confirm that the introduction of additional atoms on the Cu surface is beneficial to improve the *COOH and *CO binding strength and ultimately improve the catalytic activity. Among them, Cu-based SAAs formed by silicon and phosphorous were predicted to be the best choice for the formation of *CO intermediates (Fig. 8g). Likewise, based on first-principles calculations, Du et al. took copper (211) as a model and systematically studied the ECR activity after doping 11 different metals into Cu.[115] Fig. 8h displays the isosurface of the charge density difference for CO_2 adsorbed on Fe_1Cu (211) and Ru_1Cu (211). Theoretical calculations of the Gibbs free energy results demonstrate that Ru_1Cu (211) and Fe_1Cu (211) SAAs can break the linear relationship of the intermediate and favor the formation of CH_4 products via ECR (Fig. 8i). Similar work was reported by Lu et al., who revealed that Co_1Cu SAAs are capable of electrocatalytic conversion of CO_2 to CH_3OH.[116] A detailed free energy calculation of ECR over Co_1Cu SAAs is shown in Fig. 8j and k. The CO* desorption from the catalyst surface has a barrier of 2.25 eV, so such a process is unlikely to happen. Further electron transfer and protonation steps of *CO can obtain two possible intermediates, CHO* or COH*. On the CuCo surface, the activation energy barrier for the formation of CHO* is 1.19 eV, which is much higher than that of COH* (0.75 eV). Therefore, COH* is more likely to be formed on the CuCo alloy. In the further reduction process, the narrowed *d*-band of the Co site results in stronger bonding to COH* and CHOH* intermediates, further leading to CH_3OH. In addition, the *C intermediate is unlikely to be formed on the Co_1Cu surface due to the high endothermic energy (1.1 eV). Therefore, the authors concluded that Co_1Cu SAAs are more likely to obtain methanol rather than CH_4 at a lower overpotential.

The design principle of Cu-based SAAs can also be applied to generate C_{2+} products from ECR. Propanediol (1,2-PDO) is an important commodity chemical that can be used for producing degradable memory fibers, pharmaceutical intermediates and polymers.[117] Currently, the selective oxidation of propylene strategy is used for the production of 1, 2-PDO in industry, which is both energy and cost intensive. Thus, ECR conversion technology offers an unprecedented possibility for traditional petroleum-based processes. However, the conversion efficiency of CO_2 into 1,2-PDO via ECR technology is still low, mainly for two reasons: 1) the low rate of initial C–C bond coupling and subsequent carbon chain elongation; 2) the unclear complex reaction mechanism. Within this context, Jiao et al. carried out DFT studies and suggested that the coadsorption energy of three *CO intermediates (ΔG_{3*CO}) should be used as a descriptor for C_3 activity.[118] They adopted Ag-doped Cu SAAs (Ag_1Cu) as

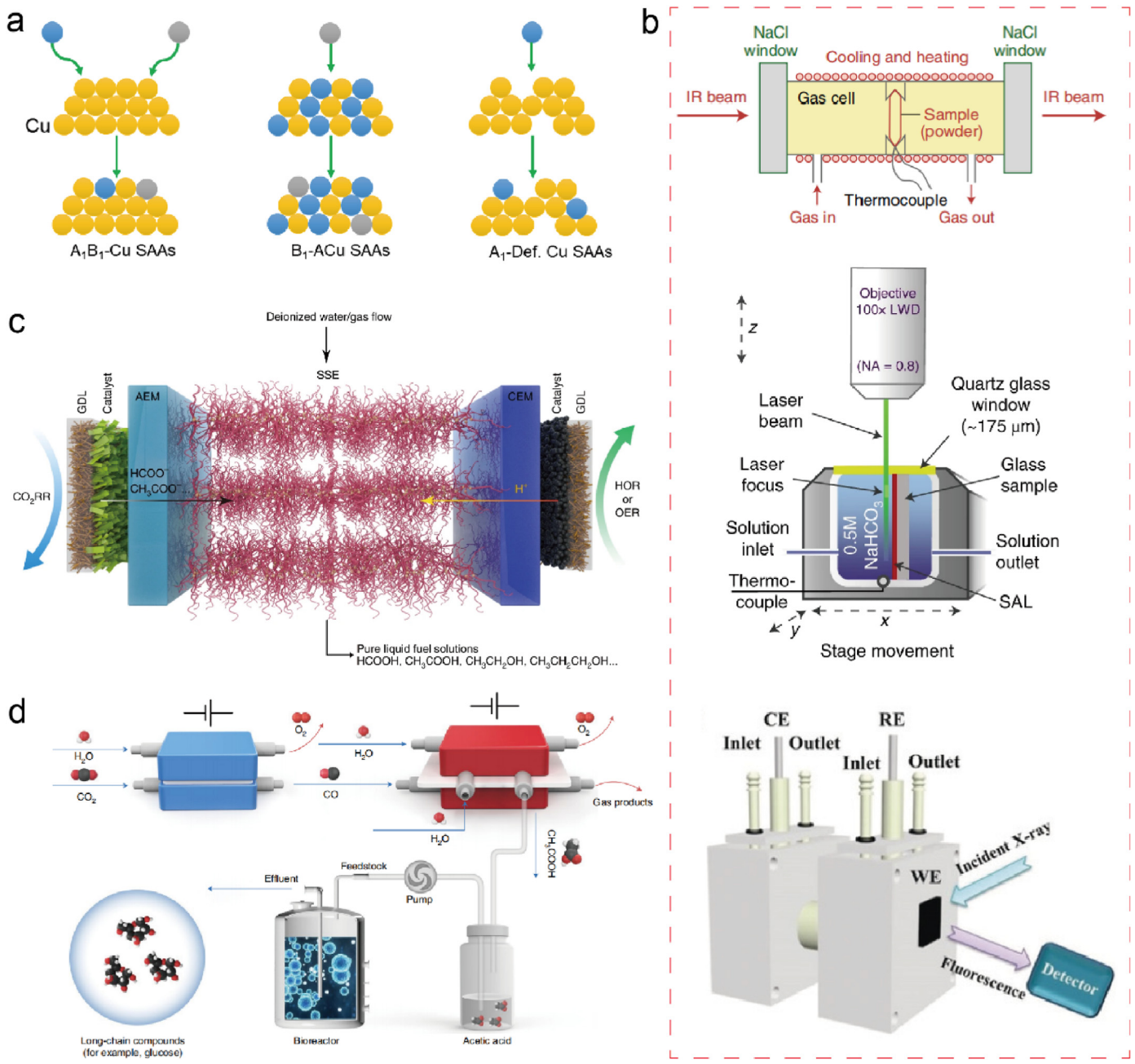

Fig. 9. (a) Schematic illustration of the future directions of highly efficient ECR catalyst preparation for Cu-based SAAs. (b) Schematic of various in-situ characterization devices (In-situ Fourier transform infrared spectroscopy; in-situ fluid-cell Raman spectroscopy; in-situ EXAFS liquid cell. Reproduced with permission from Ref. 125–127). (c) Schematic illustration of the CO_2 reduction cell with a solid electrolyte. reproduced with permission from Ref. 128. (d) Schematic illustration of the in-vitro artificial sugar synthesis system. Reproduced with permission from Ref. 129.

a model for theoretical study, demonstrating that Ag_1Cu SAAs can retain oxygen atoms in the hydroxyl group and further lead to a new C_3 product (1,2-PDO) rather than conventional n-propanol. Meanwhile, the reaction pathway of direct protonation of C to *COH–CO–CHOH (*COH–CO–COH + H^+ + e^- → *COH–CO–CHOH) facilely occurs because this process is exergonic (−0.12 eV) and thus suitable for the subsequent steps. Through the preferential protonation of C, the oxygen atoms in the hydroxyl group are perfectly preserved. Hence, 1,2-PDO can be more easily formed than other C_3 products. Alloying Cu with different metal can obtain distinct reduction products. A summary of Cu-based alloy materials in this review along with their reaction conditions for ECR to various products are displayed in Table 1.

6. Summary and outlook

The ECR to valuable chemicals provides an elegant solution to the sustainable development of energy storage systems. The preparation of multifarious C_1–C_3 products, including hydrocarbons and oxygenates, has been reported by a variety of catalysts via ECR. To date, Cu has been widely identified as the most efficient metal due to its high catalytic activity and selectivity toward hydrocarbon products. However, it suffers from various issues, such as high overpotential, low selectivity and poor stability. Alloying is a useful means for adjusting the electronic properties of the active sites and thereby ideally enhancing the catalytic activity. In this review, a systematic summary of Cu-based alloys (including conventional alloys, SAAs and HEAs) for ECR is provided, with a particular

focus on an in-depth understanding of the specific product reaction mechanism and identifying the structure-activity descriptor. Although enormous progress has been realized regarding Cu-based alloy catalysts in ECR, some difficulties still exist to be addressed.

First, research on SAAs or HEAs applied in the ECR field is still in its infancy, and both opportunities and challenges are present. In this context, effective catalyst design strategies should be proposed and tested. (1) Most Cu-based SAA catalysts are constituted by introducing one foreign metal atom to the Cu host. However, single-site catalysts possess their own shortcomings. For example, a serious deactivation phenomenon often occurs due to the limited active sites occupied by intermediates, which are unable to drive the multielectron and multiproton transfer steps.[130–132] On this issue, constructing heteronuclear diatoms on Cu hosts with tunable geometry configurations might be a useful method. (2) Nearly all Cu-based SAA catalysts in ECR contain monometallic Cu as the host metal, and it is expected that constructing SAA catalysts *via* bimetallic or polymetallic hosts might endow more adjustable electronic structures. (3) Defects can also be invoked as active sites to tune the electronic and surface properties of nanocatalysts.[133–135] On the other hand, introducing foreign atoms in the defect-rich metal Cu host and the coordinatively unsaturated metal atoms are deemed to be active sites. (4) New Cu-based HEA catalysts with large surface areas, adjustable active sites and superconductivity are promising candidates for ECR to yield some unexpected results.

Second, whether in conventional alloys, SAA or HEAs, the regulatory mechanism of foreign atom tuning on Cu is still unclear. The critical reaction intermediates and corresponding adsorption configurations in ECR are blurry. Therefore, combining multiple in -situ characterization techniques to explore the intrinsic mechanism of Cu-based alloy catalysts in ECR is necessary. For instance, in-situ X-ray diffraction (XRD) can be applied to reveal the phase transition process. In-situ ATR-FTIR and in-situ Raman reveal the adsorption configuration, intermediate formation process and desorption behavior of the final products (Fig. 9b).[125,126] The valence, bond length and coordination structure changes of Cu or other metals can be explored by in-situ X-ray absorption spectroscopy (XAS) (Fig. 9b bottom).[127] As a complementary tool, theoretical calculations can be used to reveal the intrinsic reaction mechanism.

Third, the low water solubility of CO_2 and slow mass transfer process in traditional H-type electrolytic cells severely restrict the product formation rate. In contrast, flow cells with gas diffusion electrode (GDE) can separate the gas and the liquid cavity, whereby this unique structural configuration enables the diffusion of CO_2 across the gas-liquid interface. As such, the slow mass transfer problem of CO_2 in aqueous solution can be solved. Although the developed GDE flow-cell electrolytic cell greatly improves the ECR reactivity, the solid-liquid-gas three-phase interface in the flow cell is easily “flooded” under high voltage. In addition, the generated liquid product (e.g., HCCOH, CH_3COOH, CH_3OH, etc.) via ECR are usually mixed with electrolytes such as $KHCO_3$ in both H-cell and flow-cell devices, and downstream separation steps are necessary to obtain pure products. Therefore, directly preparing high-purity and high-concentration liquid solutions is highly desirable for commercial applications. On this issue, a novel solid-electrolyte reactor has been developed, realizing the direct and continuous production of pure liquid HCOOH solutions (Fig. 9c).[128]

Finally, with the current ECR technology, the obtained products are mainly limited to C_1 or C_2 oxygenates and hydrocarbons. Nevertheless, upcycling CO_2 into energy-rich long-chain compounds with high economic value remains a huge challenge.[136,137] Recently, our group reported a hybrid electrobiosystem that combined ECR technology with yeast fermentation to efficiently convert CO_2 to glucose with a high yield (Fig. 9d).[129] This novel strategy, combining ECR and microbial fermentation technology, can also be extended to yield many valuable long-chain carbohydrates. In addition, the traditional oxygen evolution reaction (OER) can be substituted by other electrooxidations of organic molecule reactions with higher economic value. By this means, the economy of the whole system will be further improved.

In summary, although exciting advances have been achieved for Cu-based alloy catalysts in ECR, there remains enormous challenges and opportunities for future studies. The progress trend having been observed thus far for Cu-based alloys indicates that this is an emerging platform with great promise for generating valuable products via ECR with the prospect of sustainable CO_2 upcycling. It is firmly believed that through the constant efforts on both catalyst optimization and device engineering, along with the integration of in-situ characterization techniques and theoretical studies, industrial applications of ECR will be under way.

Declaration of competing interest

The authors declare no competing financial interests.

Acknowledgments

C.X. acknowledges the National Natural Science Foundation of China (NSFC 22102018 and 52171201), the Natural Science Foundation of Sichuan Province (2022NSFSC0194), the Central Government Funds of Guiding Local Scientific and Technological Development for Sichuan Province (2021ZYD0043), the University of Electronic Science and Technology of China for Startup Funding (A1098531023601264), and the Hefei National Research Center for Physical Sciences at the Microscale (KF2021005). Q.J. acknowledges the China Postdoctoral Science Foundation funded project (2022M710601) and the University of Electronic Science and Technology of China for Startup Funding (Y030212059003039). T.Z. acknowledges the NSFC (22005291 and 22278067) and University of Electronic Science and Technology of China for Startup Funding (A1098531023601356).

References

1. Gattuso JP, Magnan A, Billé R, et al. Contrasting futures for ocean and society from different anthropogenic CO_2 emissions scenarios. *Science*. 2015;349(6243):aac4722.
2. Shakun JD, Clark PU, He F, et al. Global warming preceded by increasing carbon dioxide concentrations during the last deglaciation. *Nature*. 2012;484(7392):49–54.
3. Montoya JH, Seitz LC, Chakthranont P, et al. Materials for solar fuels and chemicals. *Nat Mater*. 2016;16(1):70–81.
4. Chu S, Majumdar A. Opportunities and challenges for a sustainable energy future. *Nature*. 2012;488(7411):294–303.
5. Hasani A, Teklagne MA, Do HH, et al. Graphene-based catalysts for electrochemical carbon dioxide reduction. *Carbon Energy*. 2020;2(2):158–175.
6. Haszeldine RS, Flude S, Johnson G, et al. Negative emissions technologies and carbon capture and storage to achieve the Paris Agreement commitments. *Philos Trans A Math Phys Eng Sci*. 2018;376(2119), 20160447.
7. Wang C, Fang W, Liu Z, et al. Fischer-Tropsch synthesis to olefins boosted by MFI zeolite nanosheets. *Nat Nanotechnol*. 2022;17(7):714–720.
8. Yang HB, Hung SF, Liu S, et al. Atomically dispersed Ni(i) as the active site for electrochemical CO_2 reduction. *Nat Energy*. 2018;3(2):140–147.
9. Gao S, Lin Y, Jiao X, et al. Partially oxidized atomic cobalt layers for carbon dioxide electroreduction to liquid fuel. *Nature*. 2016;529(7584):68–71.
10. Fu X, Wang J, Hu X, et al. Scalable chemical interface confinement reduction BiOBr to bismuth porous nanosheets for electroreduction of carbon dioxide to liquid fuel. *Adv Funct Mater*. 2021;32(10).
11. Ren D, Gao J, Pan L, et al. Atomic layer deposition of ZnO on CuO enables selective and efficient electroreduction of carbon dioxide to liquid fuels. *Angew Chem Int Ed*. 2019;58(42):15036–15040.
12. Li J, Kuang Y, Meng Y, et al. Electroreduction of CO_2 to formate on a copper-based electrocatalyst at high pressures with high energy conversion efficiency. *J Am Chem Soc*. 2020;142(16):7276–7282.

13. Nitopi S, Bertheussen E, Scott SB, et al. Progress and perspectives of electrochemical CO_2 reduction on copper in aqueous electrolyte. *Chem Rev*. 2019;119(12):7610–7672.
14. Yang PP, Zhang XL, Gao FY, et al. Protecting copper oxidation state via intermediate confinement for selective CO_2 electroreduction to C_{2+} fuels. *J Am Chem Soc*. 2020;142(13):6400–6408.
15. Liu W, Zhai P, Li A, et al. Electrochemical CO_2 reduction to ethylene by ultrathin CuO nanoplate arrays. *Nat Commun*. 2022;13(1):1877.
16. Zhu Q, Sun X, Yang D, et al. Carbon dioxide electroreduction to C_2 products over copper-cuprous oxide derived from electrosynthesized copper complex. *Nat Commun*. 2019;10(1):3851.
17. Fan L, Liu CY, Zhu P, et al. Proton sponge promotion of electrochemical CO_2 reduction to multi-carbon products. *Joule*. 2022;6(1):205–220.
18. Peng C, Luo G, Zhang J, et al. Double sulfur vacancies by lithium tuning enhance CO_2 electroreduction to n-propanol. *Nat Commun*. 2021;12(1):1580.
19. Kuhl KP, Cave ER, Abram DN, et al. New insights into the electrochemical reduction of carbon dioxide on metallic copper surfaces. *Energy Environ Sci*. 2012;5(5):7050–7059.
20. Cadenhead DA, Masse NG. *The microcatalytic hydrogenation of benzene over groups VIII and Ib metals and alloys*. 1966;70(11):3558–3566.
21. Morimoto M, Takatsuji Y, Iikubo S, et al. Experimental and theoretical elucidation of electrochemical CO_2 reduction on an electrodeposited Cu_3Sn alloy. *J Phys Chem C*. 2019;123(5):3004–3010.
22. Guo X, Zhang Y, Deng C, et al. Composition dependent activity of Cu-Pt nanocrystals for electrochemical reduction of CO_2. *Chem Commun*. 2015;51(7):1345–1348.
23. Vasileff A, Xu C, Jiao Y, et al. Surface and interface engineering in copper-based bimetallic materials for selective CO_2 electroreduction. *Chem*. 2018;4(8):1809–1831.
24. Zhang M, Zhang Z, Zhao Z, et al. Tunable selectivity for electrochemical CO_2 reduction by bimetallic Cu-Sn catalysts: elucidating the roles of Cu and Sn. *ACS Catal*. 2021;11(17):11103–11108.
25. Xie P, Yao Y, Huang Z, et al. Highly efficient decomposition of ammonia using high-entropy alloy catalysts. *Nat Commun*. 2019;10(1):4011.
26. Yu Y, Xia F, Wang C, et al. High-entropy alloy nanoparticles as a promising electrocatalyst to enhance activity and durability for oxygen reduction. *Nano Res*. 2022;15(9):7868–7876.
27. Fu X, Zhang J, Zhan S, et al. High-entropy alloy nanosheets for fine-tuning hydrogen evolution. *ACS Catal*. 2022;12(19):11955–11959.
28. Yao Y, Huang Z, Xie P, et al. Carbothermal shock synthesis of high-entropy-alloy nanoparticles. *Science*. 2018;359(6383):1489–1494.
29. Yao Y, Liu Z, Xie P, et al. Computationally aided, entropy-driven synthesis of highly efficient and durable multi-elemental alloy catalysts. *Sci Adv*. 2020;6(11):eaaz0510.
30. Jørgensen M, Grönbeck H. Selective acetylene hydrogenation over single-atom alloy nanoparticles by kinetic Monte Carlo. *J Am Chem Soc*. 2019;141(21):8541–8549.
31. Zhang X, Cui G, Feng H, et al. Platinum-copper single atom alloy catalysts with high performance towards glycerol hydrogenolysis. *Nat Commun*. 2019;10(1):5812.
32. Marcinkowski MD, Darby MT, Liu J, et al. Pt/Cu single-atom alloys as coke-resistant catalysts for efficient C-H activation. *Nat Chem*. 2018;10(3):325–332.
33. Shan J, Liu J, Li M, et al. NiCu single atom alloys catalyze the C-H bond activation in the selective non-oxidative ethanol dehydrogenation reaction. *Appl Catal, B*. 2018;226:534–543.
34. Yao Y, Hu S, Chen W, et al. Engineering the electronic structure of single atom Ru sites via compressive strain boosts acidic water oxidation electrocatalysis. *Nat Catal*. 2019;2(4):304–313.
35. Duchesne PN, Li ZY, Deming CP, et al. Golden single-atomic-site platinum electrocatalysts. *Nat Mater*. 2018;17(11):1033–1039.
36. Marcinkowski MD, Liu J, Murphy CJ, et al. Selective formic acid dehydrogenation on Pt-Cu single-atom alloys. *ACS Catal*. 2016;7(1):413–420.
37. Chen CH, Wu D, Li Z, et al. Ruthenium-based single-atom alloy with high electrocatalytic activity for hydrogen evolution. *Adv Energy Mater*. 2019;9(20),1803913.
38. Yamada T, Kojima T, Abe E, et al. Probing single Pt atoms in complex intermetallic $Al_{13}Fe_4$. *J Am Chem Soc*. 2018;140(11):3838–3841.
39. Lu Q, Rosen J, Zhou Y, et al. A selective and efficient electrocatalyst for carbon dioxide reduction. *Nat Commun*. 2014;5:3242.
40. Zheng T, Jiang K, Wang H. Recent advances in electrochemical CO_2-to-CO conversion on heterogeneous catalysts. *Adv Mater*. 2018;30(48), e1802066.
41. Jin S, Hao Z, Zhang K, et al. Advances and challenges for the electrochemical reduction of CO_2 to CO: from fundamentals to industrialization. *Angew Chem Int Ed*. 2021;60(38):20627–20648.
42. Feaster JT, Shi C, Cave ER, et al. Understanding selectivity for the electrochemical reduction of carbon dioxide to formic acid and carbon monoxide on metal electrodes. *ACS Catal*. 2017;7(7):4822–4827.
43. Chen Y, Kanan MW. Tin oxide dependence of the CO_2 reduction efficiency on tin electrodes and enhanced activity for tin/tin oxide thin-film catalysts. *J Am Chem Soc*. 2012;134(4):1986–1989.
44. Xu Y, Li F, Xu A, et al. Low coordination number copper catalysts for electrochemical CO_2 methanation in a membrane electrode assembly. *Nat Commun*. 2021;12(1):2932.
45. Peterson AA, Abild-Pedersen F, Studt F, et al. How copper catalyzes the electroreduction of carbon dioxide into hydrocarbon fuels. *Energy Environ Sci*. 2010;3(9):1311–1315.
46. Yang H, Wu Y, Li G, et al. Scalable production of efficient single-atom copper decorated carbon membranes for CO_2 electroreduction to methanol. *J Am Chem Soc*. 2019;141(32):12717–12723.
47. Liu X, Li BQ, Ni B, et al. A perspective on the electrocatalytic conversion of carbon dioxide to methanol with metallomacrocyclic catalysts. *J Energy Chem*. 2022;64:263–275.
48. Zheng Y, Vasileff A, Zhou X, et al. Understanding the roadmap for electrochemical reduction of CO_2 to multi-carbon oxygenates and hydrocarbons on copper-based catalysts. *J Am Chem Soc*. 2019;141(19):7646–7659.
49. Fan L, Xia C, Yang F, et al. Strategies in catalysts and electrolyzer design for electrochemical CO_2 reduction toward C_{2+} products. *Sci Adv*. 2020;6(8), eaay3111.
50. Sun Z, Ma T, Tao H, et al. Fundamentals and challenges of electrochemical CO_2 reduction using two-dimensional materials. *Chem*. 2017;3(4):560–587.
51. Hanselman S, Koper MTM, Calle-Vallejo F. Computational comparison of late transition metal (100) surfaces for the electrocatalytic reduction of CO to C_2 species. *ACS Energy Lett*. 2018;3(5):1062–1067.
52. Hahn C, Hatsukade T, Kim YG, et al. Engineering Cu surfaces for the electrocatalytic conversion of CO_2: controlling selectivity toward oxygenates and hydrocarbons. *P Natl Acad Sci USA*. 2017;114(23):5918–5923.
53. Ren D, Wong NT, Handoko AD, et al. Mechanistic insights into the enhanced activity and stability of agglomerated Cu nanocrystals for the electrochemical reduction of carbon dioxide to n-propanol. *J Phys Chem Lett*. 2016;7(1):20–24.
54. Hori Y, Takahashi R, Yoshinami Y, et al. Electrochemical reduction of CO at a copper electrode. *J Phys Chem B*. 1997;101(36):7075–7081.
55. Hoang TTH, Verma S, Ma S, et al. Nanoporous copper-silver alloys by additive-controlled electrodeposition for the selective electroreduction of CO_2 to ethylene and ethanol. *J Am Chem Soc*. 2018;140(17):5791–5797.
56. Clark EL, Hahn C, Jaramillo TF, et al. Electrochemical CO_2 reduction over compressively strained CuAg surface alloys with enhanced multi-carbon oxygenate selectivity. *J Am Chem Soc*. 2017;139(44):15848–15857.
57. Li YC, Wang Z, Yuan T, et al. Binding site diversity promotes CO_2 electroreduction to ethanol. *J Am Chem Soc*. 2019;141(21):8584–8591.
58. Lv X, Shang L, Zhou S, et al. Electron-deficient Cu sites on Cu_3Ag_1 catalyst promoting CO_2 electroreduction to alcohols. *Adv Energy Mater*. 2020;10(37),2001987.
59. Birdja YY, Pérez-Gallent E, Figueiredo MC, et al. Advances and challenges in understanding the electrocatalytic conversion of carbon dioxide to fuels. *Nat Energy*. 2019;4(9):732–745.
60. Song Y, Chen W, Zhao C, et al. Metal-free nitrogen-doped mesoporous carbon for electroreduction of CO_2 to ethanol. *Angew Chem Int Ed*. 2017;56(36):10840–10844.
61. Duan YX, Meng FL, Liu KH, et al. Amorphizing of Cu nanoparticles toward highly efficient and robust electrocatalyst for CO_2 reduction to liquid fuels with high faradaic efficiencies. *Adv Mater*. 2018;30(14), e1706194.
62. Li F, Li YC, Wang Z, et al. Cooperative CO_2-to-ethanol conversion via enriched intermediates at molecule-metal catalyst interfaces. *Nat Catal*. 2019;3(1):75–82.
63. Karapinar D, Huan NT, Ranjbar Sahraie N, et al. Electroreduction of CO_2 on single-site copper-nitrogen-doped carbon material: selective formation of ethanol and reversible restructuration of the metal sites. *Angew Chem Int Ed*. 2019;58(42):15098–15103.
64. Ledezma-Yanez I, Gallent EP, Koper MTM, et al. Structure-sensitive electroreduction of acetaldehyde to ethanol on copper and its mechanistic implications for CO and CO_2 reduction. *Catal Today*. 2016;262:90–94.
65. Vasileff A, Xu C, Jiao Y, et al. Surface and interface engineering in copper-based bimetallic materials for selective CO_2 electroreduction. *Chem*. 2018;4(8):1809–1831.
66. Zheng T, Jiang K, Ta N, et al. Large-scale and highly selective CO_2 electrocatalytic reduction on nickel single-atom catalyst. *Joule*. 2019;3(1):265–278.
67. Shang H, Sun W, Sui R, et al. Engineering isolated Mn-N_2C_2 atomic interface sites for efficient bifunctional oxygen reduction and evolution reaction. *Nano Lett*. 2020;20(7):5443–5450.
68. Kim D, Xie C, Becknell N, et al. Electrochemical activation of CO_2 through atomic ordering transformations of AuCu nanoparticles. *J Am Chem Soc*. 2017;139(24):8329–8336.
69. Kim D, Resasco J, Yu Y, et al. Synergistic geometric and electronic effects for electrochemical reduction of carbon dioxide using gold-copper bimetallic nanoparticles. *Nat Commun*. 2014;5:4948.
70. Wang G, Li X, Yang X, et al. Metal-based aerogels catalysts for electrocatalytic CO_2 reduction. *Chem Eur J*. 2022, e202201834.
71. Zhong D, Zhang L, Zhao Q, et al. Concentrating and activating carbon dioxide over AuCu aerogel grain boundaries. *J Chem Phys*. 2020;152(20), 204703.
72. An C, Shen Y, Yan W, et al. Surface-tuning nanoporous $AuCu_3$ engineering syngas proportion by electrochemical conversion of CO_2. *Nano Res*. 2021;14(11):3907–3912.
73. Zhou R, Fan X, Ke X, et al. Two-dimensional palladium-copper alloy nanodendrites for highly stable and selective electrochemical formate production. *Nano Lett*. 2021;21(9):4092–4098.
74. Gao D, Zhou H, Cai F, et al. Pd-containing nanostructures for electrochemical CO_2 reduction reaction. *ACS Catal*. 2018;8(2):1510–1519.
75. Mun Y, Lee S, Cho A, et al. Cu-Pd alloy nanoparticles as highly selective catalysts for efficient electrochemical reduction of CO_2 to CO. *Appl Catal, B*. 2019;246:82–88.
76. Li M, Wang J, Li P, et al. Mesoporous palladium-copper bimetallic electrodes for selective electrocatalytic reduction of aqueous CO_2 to CO. *J Mater Chem A*. 2016;4(13):4776–4782.
77. Duan YX, Zhou YT, Yu Z, et al. Boosting production of HCOOH from CO_2 electroreduction via Bi/CeO_x. *Angew Chem Int Ed*. 2021;60(16):8798–8802.

78. Liu S, Xiao J, Lu XF, et al. Efficient electrochemical reduction of CO_2 to HCOOH over Sub-2 nm SnO_2 quantum wires with exposed grain boundaries. *Angew Chem Int Ed*. 2019;58(25):8499–8503.
79. Gupta K, Bersani M, Darr JA. Highly efficient electro-reduction of CO_2 to formic acid by nano-copper. *J Mater Chem A*. 2016;4(36):13786–13794.
80. Duarah P, Haldar D, Yadav VSK, et al. Progress in the electrochemical reduction of CO_2 to formic acid: a review on current trends and future prospects. *J Environ Chem Eng*. 2021;9(6), 106394.
81. Wang HH, Zhang SN, Zhao TJ, et al. Mild and selective hydrogenation of CO_2 into formic acid over electron-rich MoC nanocatalysts. *Sci Bull*. 2020;65(8):651–657.
82. Lv H, Lv F, Qin H, et al. Single-crystalline mesoporous palladium and palladium-copper nanocubes for highly efficient electrochemical CO_2 reduction. *CCS Chem*. 2022;4(4):1376–1385.
83. Zhu W, Zhang L, Yang P, et al. Morphological and compositional design of Pd-Cu bimetallic nanocatalysts with controllable product selectivity toward CO_2 electroreduction. *Small*. 2018;14(7), 1703314.
84. Navarro-Jaén S, Virginie M, Bonin J, et al. Highlights and challenges in the selective reduction of carbon dioxide to methanol. *Nat Rev Chem*. 2021;5(8):564–579.
85. Wu Y, Jiang Z, Lu X, et al. Domino electroreduction of CO_2 to methanol on a molecular catalyst. *Nature*. 2019;575(7784):639–642.
86. Yang D, Zhu Q, Chen C, et al. Selective electroreduction of carbon dioxide to methanol on copper selenide nanocatalysts. *Nat Commun*. 2019;10(1):677.
87. Zhang W, Qin Q, Dai L, et al. Electrochemical reduction of carbon dioxide to methanol on hierarchical Pd/SnO_2 nanosheets with abundant Pd-O-Sn interfaces. *Angew Chem Int Ed*. 2018;57(30):9475–9479.
88. Bagchi D, Raj J, Singh AK, et al. Structure-tailored surface oxide on Cu-Ga intermetallics enhances CO_2 reduction selectivity to methanol at ultralow potential. *Adv Mater*. 2022;34(19), e2109426.
89. Lu L, Sun X, Ma J, et al. Highly efficient electroreduction of CO_2 to methanol on palladium-copper bimetallic aerogels. *Angew Chem Int Ed*. 2018;57(43):14149–14153.
90. Pang Y, Li J, Wang Z, et al. Efficient electrocatalytic conversion of carbon monoxide to propanol using fragmented copper. *Nat Catal*. 2019;2(3):251–258.
91. Zhuang TT, Pang Y, Liang ZQ, et al. Copper nanocavities confine intermediates for efficient electrosynthesis of C_3 alcohol fuels from carbon monoxide. *Nat Catal*. 2018;1(12):946–951.
92. Wang X, Wang Z, Zhuang TT, et al. Efficient upgrading of CO to C_3 fuel using asymmetric C-C coupling active sites. *Nat Commun*. 2019;10(1):5186.
93. Wang X, Ou P, Ozden A, et al. Efficient electrosynthesis of n-propanol from carbon monoxide using a Ag-Ru-Cu catalyst. *Nat Energy*. 2022;7(2):170–176.
94. Rahaman M, Kiran K, Montiel IZ, et al. Selective n-propanol formation from CO_2 over degradation-resistant activated PdCu alloy foam electrocatalysts. *Green Chem*. 2020;22(19):6497–6509.
95. Jiang X, Cai F, Gao D, et al. Electrocatalytic reduction of carbon dioxide over reduced nanoporous zinc oxide. *Eletrochem Commun*. 2016;68:67–70.
96. Feng Y, Li Z, Liu H, et al. Laser-prepared CuZn alloy catalyst for selective electrochemical reduction of CO_2 to ethylene. *Langmuir*. 2018;34(45):13544–13549.
97. Su X, Sun Y, Jin L, et al. Hierarchically porous Cu/Zn bimetallic catalysts for highly selective CO_2 electroreduction to liquid C_2 products. *Appl Catal, B*. 2020;269, 118800.
98. Shang L, Lv X, Zhong L, et al. Efficient CO_2 electroreduction to ethanol by Cu_3Sn catalyst. *Small Methods*. 2022;6(2), e2101334.
99. Wu D, Kusada K, Yamamoto T, et al. Platinum-group-metal high-entropy-alloy nanoparticles. *J Am Chem Soc*. 2020;142(32):13833–13838.
100. Qiao H, Saray MT, Wang X, et al. Scalable synthesis of high entropy alloy nanoparticles by microwave heating. *ACS Nano*. 2021;15(9):14928–14937.
101. Qiu XW, Zhang YP, He L, et al. Microstructure and corrosion resistance of AlCrFeCuCo high entropy alloy. *J Alloy Compo*. 2013;549:195–199.
102. Murty BS, Yeh JW, Ranganathan S, et al. *High-entropy Alloys*. Elsevier; 2019.
103. Xin Y, Li S, Qian Y, et al. High-entropy alloys as a platform for catalysis: progress, challenges, and opportunities. *ACS Catal*. 2020;10(19):11280–11306.
104. Lv ZY, Liu XJ, Jia B, et al. Development of a novel high-entropy alloy with eminent efficiency of degrading azo dye solutions. *Sci Rep*. 2016;6(1):1–11.
105. Nellaiappan S, Katiyar NK, Kumar R, et al. High-entropy alloys as catalysts for the CO_2 and CO reduction reactions: experimental realization. *ACS Catal*. 2020;10(6):3658–3663.
106. Li H, Huang H, Chen Y, et al. High-entropy alloy aerogels: a new platform for carbon dioxide reduction. *Adv Mater*. 2022;2209242:1–16.
107. Pedersen JK, Batchelor TAA, Bagger A, et al. High-entropy alloys as catalysts for the CO_2 and CO reduction reactions. *ACS Catal*. 2020;10(3):2169–2176.
108. Liu J, Lucci FR, Yang M, et al. Tackling CO poisoning with single-atom alloy catalysts. *J Am Chem Soc*. 2016;138(20):6396–6399.
109. Papanikolaou KG, Darby MT, Stamatakis M. Engineering the surface architecture of highly dilute alloys: an ab initio Monte Carlo approach. *ACS Catal*. 2019;10(2):1224–1236.
110. Tierney HL, Baber AE, Sykes ECH. Atomic-scale imaging and electronic structure determination of catalytic sites on Pd/Cu near surface alloys. *J Phys Chem C*. 2009;113(17):7246–7250.
111. Hannagan RT, Patel DA, Cramer LA, et al. Combining STM, RAIRS and TPD to decipher the dispersion and interactions between active sites in RhCu single-atom alloys. *ChemCatChem*. 2020;12(2):488–493.
112. Ren W, Tan X, Qu J, et al. Isolated copper-tin atomic interfaces tuning electrocatalytic CO_2 conversion. *Nat Commun*. 2021;12(1):1449.
113. Zheng T, Liu C, Guo C, et al. Copper-catalysed exclusive CO_2 to pure formic acid conversion via single-atom alloying. *Nat Nanotechnol*. 2021;16(12):1386–1393.
114. Wang D, Cao R, Hao S, et al. Accelerated prediction of Cu-based single-atom alloy catalysts for CO_2 reduction by machine learning. *Green Energy Environ*. 2021;20(4):468–472.
115. Feng Y, An W, Wang Z, et al. Electrochemical CO_2 reduction reaction on M@Cu(211) bimetallic single-atom surface alloys: mechanism, kinetics, and catalyst screening. *ACS Sustainable Chem Eng*. 2019;8(1):210–222.
116. Zhao Z, Lu G. Cu-based single-atom catalysts boost electroreduction of CO_2 to CH_3OH: first-principles predictions. *J Phys Chem C*. 2019;123(7):4380–4387.
117. Zhang X, Cui G, Wei M. PtIn alloy catalysts toward selective hydrogenolysis of glycerol to 1,2-Propanediol. *Ind Eng Chem Res*. 2020;59(29):12999–13006.
118. Chen L, Tang C, Zheng Y, et al. C_3 production from CO_2 reduction by concerted *CO trimerization on a single-atom alloy catalyst. *J Mater Chem A*. 2022;10(11):5998–6006.
119. Rasul S, Anjum DH, Jedidi A, et al. A highly selective copper-indium bimetallic electrocatalyst for the electrochemical reduction of aqueous CO_2 to CO. *Angew Chem Int Ed*. 2015;54(7):2146–2150.
120. Sun Y, Wang F, Liu F, et al. Accelerating Pd electrocatalysis for CO_2-to-formate conversion across a wide potential window by optimized incorporation of Cu. *ACS Appl Mater Interfaces*. 2022;14(7):8896–8905.
121. Ye K, Cao A, Shao J, et al. Synergy effects on Sn-Cu alloy catalyst for efficient CO_2 electroreduction to formate with high mass activity. *Sci Bull*. 2020;65(9):711–719.
122. Wei B, Xiong Y, Zhang Z, et al. Efficient electrocatalytic reduction of CO_2 to HCOOH by bimetallic In-Cu nanoparticles with controlled growth facet. *Appl Catal, B*. 2021;283, 119646.
123. Bernal M, Bagger A, Scholten F, et al. CO_2 electroreduction on copper-cobalt nanoparticles: size and composition effect. *Nano Energy*. 2018;53:27–36.
124. Jia S, Zhu Q, Wu H, et al. Efficient electrocatalytic reduction of carbon dioxide to ethylene on copper–antimony bimetallic alloy catalyst. *Chin J Catal*. 2020;41(7):1091–1098.
125. Handoko AD, Wei F, Yeo BS, et al. Understanding heterogeneous electrocatalytic carbon dioxide reduction through operando techniques. *Nat Catal*. 2018;1(12):922–934.
126. Geisler T, Dohmen L, Lenting C, et al. Real-time in situ observations of reaction and transport phenomena during silicate glass corrosion by fluid-cell Raman spectroscopy. *Nat Mater*. 2019;18(4):342–348.
127. Ye K, Zhou Z, Shao J, et al. In situ reconstruction of a hierarchical Sn-Cu/SnO_x core/shell catalyst for high-performance CO_2 electroreduction. *Angew Chem Int Ed*. 2020;59(12):4814–4821.
128. Xia C, Zhu P, Jiang Q, et al. Continuous production of pure liquid fuel solutions via electrocatalytic CO_2 reduction using solid-electrolyte devices. *Nat Energy*. 2019;4(9):776–785.
129. Zheng T, Zhang M, Wu L, et al. Upcycling CO_2 into energy-rich long-chain compounds via electrochemical and metabolic engineering. *Nat Catal*. 2022;5(5):388–396.
130. Zhang W, Chao Y, Zhang W, et al. Emerging dual-atomic-site catalysts for efficient energy catalysis. *Adv Mater*. 2021;33(36), e2102576.
131. Ouyang Y, Shi L, Bai X, et al. Breaking scaling relations for efficient CO_2 electrochemical reduction through dual-atom catalysts. *Chem Sci*. 2020;11(7):1807–1813.
132. Chen Z, Su X, Ding J, et al. Boosting oxygen reduction reaction with Fe and Se dual-atom sites supported by nitrogen-doped porous carbon. *Appl Catal, B*. 2022;308, 121206.
133. Yan D, Li Y, Huo J, et al. Defect chemistry of nonprecious-metal electrocatalysts for oxygen reactions. *Adv Mater*. 2017;29(48), 1606459.
134. Xie J, Zhang H, Li S, et al. Defect-rich MoS_2 ultrathin nanosheets with additional active edge sites for enhanced electrocatalytic hydrogen evolution. *Adv Mater*. 2013;25(40):5807–5813.
135. Zhang B, Zhang J, Hua M, et al. Highly electrocatalytic ethylene production from CO_2 on nanodefective Cu nanosheets. *J Am Chem Soc*. 2020;142(31):13606–13613.
136. O'Brien CP, Watson MJ, Dowling AW. Challenges and opportunities in converting CO_2 to carbohydrates. *ACS Energy Lett*. 2022;7(10):3509–3523.
137. Hann EC, Overa S, Harland-Dunaway M, et al. A hybrid inorganic-biological artificial photosynthesis system for energy-efficient food production. *Nat Food*. 2022;3(6):461–471.

Ding Mao is currently working toward her undergraduate degree in the Department of Materials and Energy at University of Electronic Science and Technology of China (UESTC). Her current research focuses on the synthesis and characterization of nanomaterials for electrocatalytic CO_2 reduction.

Zhaoyang Chen received his Ph.D. degree from Wuhan University in 2021. Now he is a postdoctoral fellow in the Department of Materials and Energy at University of Electronic Science and Technology of China (UESTC). His current research interests mainly focus on nanomaterials and catalysts for electrochemical reduction of CO_2, oxygen reduction reaction and small molecule conversion for a sustainable future.

Chuan Xia is a professor of Department of Materials and Energy at University of Electronic Science and Technology of China (UESTC). He obtained his Ph.D. degree at King Abdullah University of Science and Technology (KAUST) in 2018 followed by a post-doctoral Fellowship at Harvard University and Rice University. In 2020 he joined UESTC, where he initiated an active research group focusing on developing methods for controlling the architecture of molecules and materials, understanding their fundamental properties, and utilizing such structures to develop novel catalysts that can be applied in the areas of electrocatalysis, energy generation, storage and conversion.